Unusual properties of the RY3 center in GaN

M. A. Reshchikov,[1,*] R. M. Sayeed,[2] Ü. Özgür,[2] D. O. Demchenko,[1] J. D. McNamara,[1,†] V. Prozheeva,[3] F. Tuomisto,[3]
H. Helava,[4] A. Usikov,[4,5] and Yu. Makarov[4]

[1]*Department of Physics, Virginia Commonwealth University, Richmond, Virginia 23284, USA*
[2]*Department of Electrical and Computer Engineering, Virginia Commonwealth University, Richmond, Virginia 23284, USA*
[3]*Department of Applied Physics, Aalto University, 00076 Aalto, Finland*
[4]*Nitride Crystals, Inc., 9702 Gayton Road, Ste. 320, Richmond, Virginia 23238, USA*
[5]*Saint-Petersburg National Research University of Information Technologies, Mechanics and Optics, 49 Kronverkskiy Ave.,
197101 Saint Petersburg, Russia*

The investigation and identification of point defects in GaN is crucial for improving the reliability of light-emitting and high-power electronic devices. The RY3 defect with a characteristic emission band at about 1.8 eV is often observed in photoluminescence (PL) spectra of *n*-type GaN grown by hydride vapor phase epitaxy, and it exhibits unusual properties. Its emission band consists of two components: a fast (10-ns lifetime) RL3 with a maximum at 1.8 eV and a slow (100–300 μs lifetime) YL3 with a maximum at 2.1 eV and zero-phonon line at 2.36 eV. In steady-state PL measurements, the YL3 component emerges with increasing temperature from 90 to 180 K, concurrently with a decrease in the RL3 intensity. The activation energy of both processes is about 0.06 eV. In time-resolved PL, the YL3 intensity abruptly rises when the RL3 intensity begins to saturate. These and other phenomena can be explained using a model of an acceptor with two excited states. A delocalized, effective-mass state at about 0.2 eV above the valence band captures photogenerated holes. These holes transition to the ground state, which produces the RL3 component with a lifetime of ∼10 ns. Alternatively, they may nonradiatively transition over a 0.06 eV-high barrier to a localized excited state with a level at 1.13 eV above the valence band. Recombination of free electrons or electrons at shallow donors with the holes at this localized excited state is responsible for the YL3 component. The relative intensities of the RL3 and YL3 components are dictated by the probabilities of holes at the shallow excited state to transition to the ground or to the localized excited states. Transition metals and complex defects are considered as the main candidates for the RY3 center.

I. INTRODUCTION

In the history of point defects in semiconductors, there are a few cases that have attracted significant attention due to unusual properties of a defect and its potential importance for semiconductor applications. Among these are the NV (nitrogen-vacancy) center in diamond [1] and the DX and EL2 centers in GaAs attributed to the Si_{Ga} and As_{Ga} antisite-containing defects, respectively [2,3]. Understanding the properties and behavior of defects with unusual properties also advances developments in the theory of point defects in semiconductors. Currently, GaN is attracting significant attention due to its applications in light-emitting and high-power electronic devices. Point defects in GaN have been extensively studied in the last 2–3 decades, yet many questions regarding the origin and behavior of deep-level defects remain unanswered. The most popular and thoroughly studied defect in GaN is carbon, which is responsible for the yellow luminescence (YL) band commonly observed in undoped or *n*-type doped GaN samples grown by metal-organic chemical

vapor deposition (MOCVD) [4]. Only recently, the YL band with a maximum at 2.20 eV and zero-phonon line (ZPL) at 2.59 eV (also labeled the YL1 band) has been unambiguously attributed to the isolated carbon acceptor (C_N) [5–7]. In agreement with theoretical predictions, two charge states of this defect, with the −/0 transition level at 0.916 ± 0.003 eV and the 0/+ transition level at 0.3 ± 0.1 eV above the valence band, have been detected experimentally [7,8].

Hydride vapor phase epitaxy (HVPE) is currently the most popular method for obtaining commercial-grade GaN wafers for high-power electronics. Defects in this material are less understood, although there is a strong motivation to identify and eliminate them. In undoped GaN grown by HVPE, the YL1 band is not common, because the carbon contamination is low in this growth method [4,6]. Instead, a red luminescence (RL) band with a maximum at 1.7–1.8 eV is often observed. In fact, several defects are responsible for similar RL bands near 1.8 eV in undoped GaN (Sec. IV) [4,9]. This work is devoted to the RL3 band, which is observed only in HVPE-grown GaN and characterized by a very short (about 10 ns) lifetime [10]. Due to the very fast decay and unusual shape of this PL band (a shoulder at the high-energy side), we recognize it in a variety of GaN samples grown by different groups using the HVPE method. These include very pure freestanding GaN templates grown by the Samsung Advanced Institute

---

*Corresponding author: mreschi@vcu.edu
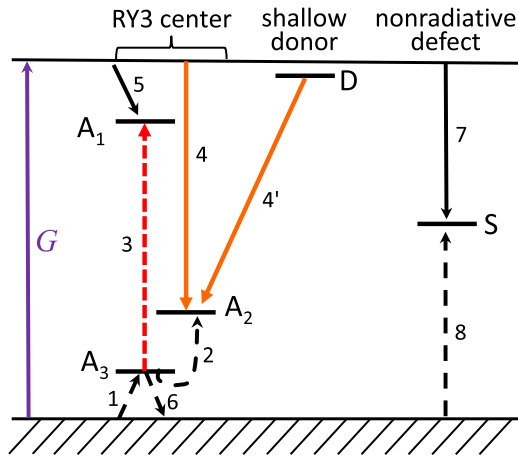†Currently at: Savannah River National Laboratory, Aiken, SC 29803.

FIG. 1. Band diagram and transitions associated with the RY3 band in GaN. A_1, A_2, and A_3 are three states of the RY3 center, where A_1 is the ground state of the acceptor, and A_2 and A_3 are excited states with a localized and delocalized hole, respectively. The electron and hole transitions are shown with solid and dashed arrows, respectively. Transition 3 is responsible for the RL3 component with a maximum at 1.8 eV. Transitions 4 and 4′ cause the YL3 component with a maximum at 2.1 eV and the ZPL at 2.36–2.38 eV. Other transitions are explained in the text.

of Technology [4], high-quality freestanding templates from Kyma Technologies, and GaN layers on sapphire substrates grown by TDI, as well as by Nitride Crystals. The RL3 band always appears together with the yellow luminescence (YL3) band, so it is impossible to resolve these bands in steady-state PL (SSPL) experiments [10–13]. Time-resolved PL (TRPL) measurements allowed us to establish that the ZPL at 2.36 eV at low temperature belongs not to the RL3 band, as was proposed earlier [11], but to the YL3 band, which has a maximum at 2.1 eV and characteristic phonon-related fine structure on its high-energy side [10]. In this work, we will show that both the RL3 and YL3 bands (called RL3 and YL3 components, hereafter) originate from the same defect, which will be called the RY3 center (also RY3 defect and RY3 band).

The RY3 defect behaves as an acceptor, and it exhibits unusual properties. According to the model proposed in this paper, it has two excited states: one (A_3) is a shallow, diffuse state with a delocalized hole, and the other (A_2) is a localized state, with a transition level at 1.13 eV above the valence band (Fig. 1). Transitions from the delocalized excited state to the localized excited state occur nonradiatively, and over a potential barrier with an effective height of about 0.06 eV. Alternatively, the hole at the delocalized state (A_3) may transition to the deep, ground state of the acceptor (A_1). This is an internal transition of the bound hole with a characteristic time of about 10 ns, which produces the RL3 component. The hole at the localized excited state (A_2) recombines radiatively with electrons at shallow donors at low temperatures, or with electrons in the conduction band at elevated temperatures. These transitions produce the YL3 component.

II. EXPERIMENTAL DETAILS

The RY3 band was reliably identified in at least 20 unintentionally doped GaN samples grown by HVPE on sapphire substrates. In particular, samples H101, H102, and H106 have a very intense RY3 band and were grown in a vertical HVPE reactor at 850 °C. Hall effect measurements showed the concentration of free electrons to be between 4×10^{16} and 8×10^{16} cm^{-3} at room temperature in these samples. Independently, the concentration of free electrons was estimated as $\sim 2 \times 10^{16}$ cm^{-3} at 250 K from TRPL.

Undoped GaN samples H201 and H202 exhibit a very weak RY3 band and were grown in a horizontal HVPE reactor at temperatures between 950 °C and 1050 °C. These are conductive *n*-type samples with a room-temperature concentration of free electrons of about 1×10^{17} cm^{-3}. Detailed growth conditions for undoped *n*-type samples T2015, RS280, and RS320 are not disclosed. The RY3 band, or at least its signature, was found in nearly all *n*-type, HVPE-grown GaN samples produced by different research groups and companies, including a Si-doped sample. However, we could not find any correlation between the growth conditions and the presence of the RY3 band.

Secondary ion mass-spectrometry (SIMS) measurements have been carried out by the Evans Analytical Group. Positron annihilation spectroscopy (PAS) experiments have been conducted to estimate the concentrations of gallium vacancies (V_{Ga}) or V_{Ga}-related complexes in the studied GaN samples. Details of the experimental approach and analyses can be found elsewhere [14,15].

PL measurements were performed using a 325-nm HeCd laser (model IK35552R-G from Kimmon Electric) for SSPL and a 337-nm nitrogen pulsed laser (model GL-3300 from Photon Technology International, 1 ns pulse duration and 6 Hz repetition frequency) for TRPL. The excitation power density P_{exc} was varied between 10^{-5} and 0.2 W/cm^2 in SSPL experiments by introducing calibrated neutral density filters in the laser beam path. The photon flux at the sample surface from the nitrogen pulsed laser was varied between 10^{17} and 5×10^{23} cm^{-2} s^{-1} using neutral density filters. The PL spectra in the photon range between 1.5 and 3.5 eV were analyzed by a grating monochromator with a focal length of 0.3 m (Triax-320 from Horiba) and detected using a cooled photomultiplier tube (Hamamatsu R928). Temperature-dependent measurements were conducted using a closed-cycle He cryostat between 18 and 320 K and in a high-temperature cryostat between 100 and 680 K (models CCS-100/202N and VPF-700, respectively, from Janis Research Company). Ultrafast PL transients were measured using 266 nm excitation from a frequency-tripled femtosecond Ti:sapphire laser (25 W/cm^2 time-average power density, 80 MHz repetition rate) and a Hamamatsu streak camera with 25-ps resolution in the photon counting mode.

Measurements were corrected for the optical elements and detector sensitivities with a calibrated tungsten-halogen lamp. The spectra measured as a function of wavelength λ were multiplied by λ^3 in order to plot the spectra in units proportional to the number of emitted photons as a function of photon energy [7]. This procedure causes a small red shift in the maxima of broad bands. For this reason, the positions of broad band maxima determined in this work and in Ref. [7] are slightly different from those in our previous publications where the spectra were not multiplied by λ^3. The absolute internal quantum efficiency of a PL band, η_i, is defined as
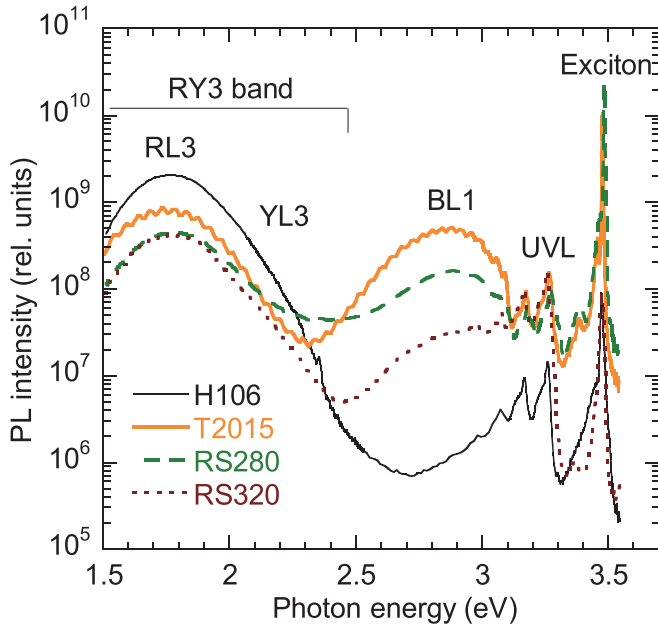
FIG. 2. Low-temperature (18 K) PL spectra for selected GaN samples at $P_{exc} \approx 10^{-4}\,\mathrm{W/cm^2}$.

FIG. 3. PL spectra at select temperatures for sample H106, at $P_{exc} = 10^{-4}\,\mathrm{W/cm^2}$.

$\eta_i = I_i^{PL}/G$, where I_i^{PL} is the PL intensity from ith type of defect (number of photons emitted from a unit volume per unit time) and G is the electron-hole generation rate for the same volume. In this work, η_i for PL bands were estimated by comparing integrated PL intensities with those obtained from calibrated GaN samples. The absolute internal quantum efficiency for the calibrated samples (such as sample MD42 in Ref. [7]) was found with a method based on a detailed analysis of PL and fitting these data with a rate-equation model [15–17].

III. EXPERIMENTAL RESULTS

A. Contributions of the RL3 and YL3 components to the RY3 band in SSPL

At $T = 18$ K, the RY3 band with a maximum at 1.77 eV and the ZPL at 2.36 eV is the strongest defect-related PL band in the set of GaN samples selected for this study (Fig. 2). The SSPL spectra from these and other samples also contain sharp excitonic lines with the strongest peak at 3.475 eV attributed to the donor-bound exciton and the $\mathrm{Mg_{Ga}}$-related ultraviolet luminescence (UVL) band with the first peak at 3.27 eV. In some samples, the $\mathrm{Zn_{Ga}}$-related blue luminescence (BL1) band with a maximum at 2.9 eV is strong, while in others it cannot be resolved at $T = 18$ K (Fig. 2). The green luminescence (GL1) band with a maximum at 2.4 eV could also be detected in most of the samples, but only at high excitation intensities due to its superlinear dependence on excitation intensity, which is orders of magnitude higher than that used to collect spectra shown in Fig. 2 [9].

With increasing temperature from 18 to 100 K, the shape of the RY3 band remains nearly unchanged, while the ZPL and phonon-related fine structure completely disappear. Select SSPL spectra at temperatures between 100 and 300 K are shown in Fig. 3. After thermal quenching of the UVL band,
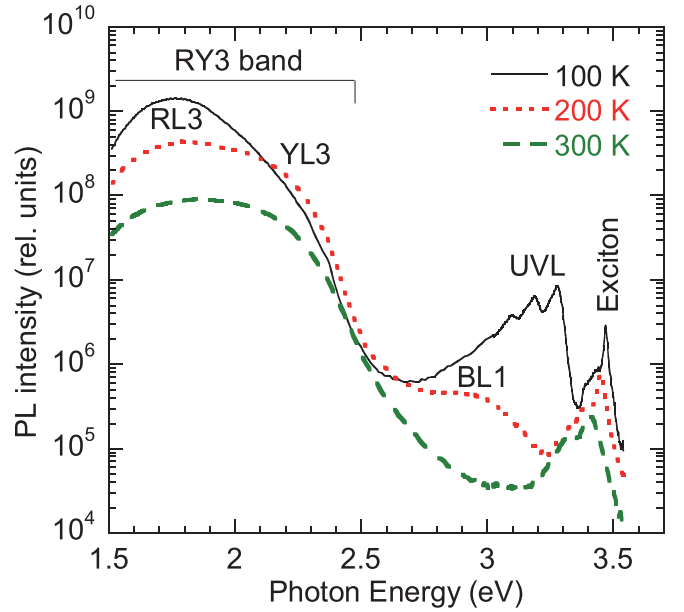
a weak broad band with a maximum at about 2.9 eV can be partially resolved at $T = 200$ K. This band is identified as the BL1 band owing to its characteristic temperature behavior and other distinguishing features [9].

As will be shown below, the RY3 band consists of two unresolved components: the RL3 with a maximum at about 1.8 eV and the YL3 with a maximum at about 2.1 eV. An interesting transformation of the RY3 band shape can be observed with increasing temperature from 100 to 200 K: the YL3 component rises while the RL3 component is quenched (Fig. 3). At higher temperatures, the shape of the RY3 band does not change significantly. The transformation of the overall band shape with temperature is identical in all samples. Unfortunately, because of the significant overlap between the RL3 and YL3 components, they cannot be reliably resolved in the SSPL spectrum.

Fortunately, the RL3 and YL3 components can be resolved in TRPL experiments, because they have very different characteristic lifetimes ($\tau^{PL} \approx 10$ ns for the RL3 component and $\tau^{PL} \approx 100 - 300\,\mu$s for the YL3 component) [10]. The shape of the fast RL3 component is better resolved at low excitation intensity (at $P_0 < 10^{20}\,\mathrm{cm^{-2}\,s^{-1}}$), when the contribution of the YL3 component is negligible (see Sec. III E). On the other hand, the shape of the slow YL3 component can be reliably found at relatively high excitation intensity ($P_0 \approx 10^{22}\,\mathrm{cm^{-2}\,s^{-1}}$) and long time delays [10]. The shapes of the fast (RL3) and slow (YL3) components of the RY3 band were carefully determined at different temperatures from TRPL spectra. Note that the shapes were identical in different samples and did not change for a wide range of excitation intensities. This made it possible to reliably resolve the broad RY3 band into the RL3 and YL3 components in the SSPL spectra at different temperatures (between 18 and 300 K) and to find their relative contributions. Examples of the RY3 band deconvolution at $T = 18$ and 180 K are shown in Fig. 4.
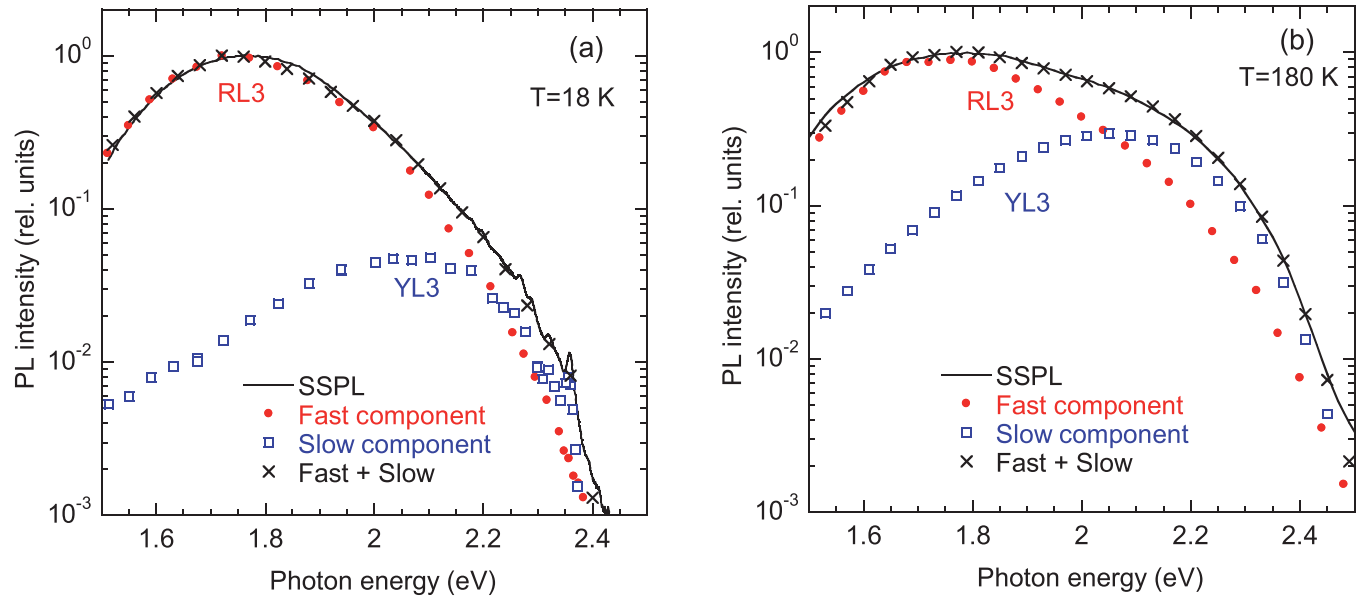
FIG. 4. The RY3 band in sample H106 at (a) $T = 18$ and (b) 180 K. The solid line is the normalized SSPL spectrum at $P_{exc} = 10^{-3}$ W/cm^2. The filled circles and empty squares show the fast (at $\sim 10^{-8}$ s) and slow (at $\sim 10^{-4}$ s) components, respectively, of the RY3 band obtained from TRPL excited with a nitrogen pulse laser. They are shifted arbitrarily in the vertical direction in a logarithmic scale, so that their sum (shown with the $\times$ symbols) matches the SSPL spectrum.

Interestingly, while the high-energy side of both components extends to ~ 2.4 eV at 18 K, only the slow YL3 component contains the ZPL at 2.36 eV [Fig. 4(a)]. The integrated PL intensity for each component i was converted to the absolute internal quantum efficiency, η_i, by using calibrated GaN samples.

B. Temperature dependence of PL intensity

The temperature dependences of the quantum efficiency, $\eta_i(T)$, for the RL3 and YL3 components in SSPL are shown in Fig. 5. It is immediately noticeable that the increase of the YL3 intensity with increasing temperature from 100 to 200 K is very unusual. One possible cause for such behavior could be thermal quenching of a very strong PL band (with internal quantum efficiency close to unity), followed by redistribution of thermally emitted holes among all other recombination channels [17,18]. An important feature of this mechanism is that the intensities of *all* PL bands, other than the band being quenched, must increase very similarly and simultaneously. For sample H106 shown in Fig. 5, the quantum efficiency of the RL3 component is indeed very high; however, the temperature dependence of the exciton band intensity does not show any increase in this temperature region (Fig. 5). Thus this mechanism is unlikely to cause the increase of the YL3 intensity.

The rise of the YL3 component occurs simultaneously with the quenching of the RL3 component and with the same activation energy for both these processes. This behavior was reproduced in all the samples where these components were intense enough to be analyzed, which suggests that both PL bands originate from the same defect (the RY3 center). The RL3 component is gradually replaced with the YL3 component with a thermal activation energy of about 0.06 eV.

The temperature dependences of η_i for the RL3 and YL3 components in the SSPL were fitted with the following empirical expression:

$$\eta_i(T) = \eta_{0i} \frac{1 + C_3 \exp\left(-E_1/kT\right)}{1 + C_1 \exp\left(-E_1/kT\right) + C_2 \exp\left(-E_2/kT\right)}, \quad (1)$$

with $C_3 = 0$ for the RL3 component. Here, η_{0i} is the quantum efficiency of the RL3 or the YL3 component in the limit of low temperatures, C_1, C_2, and C_3 are dimensionless parameters, and E_1 and E_2 are activation energies. Equation (1) is derived in the Appendix for transitions shown in Fig. 1. The PL intensities of both components are independent of temperature ($\eta_i = \eta_{0i}$) up to 90 K, since all the exponential terms are small. From 100 to 200 K, the YL3 intensity increases with an activation energy of $E_1 \approx 0.06$ eV, as the RL3 component is quenched concurrently and with the same activation energy. In this temperature region, the term with C_2 and E_2 in Eq. (1) is negligibly small. At $T > 200$ K, both components are quenched with $E_2 \approx 0.2$ eV.

At temperatures above 300 K, the RL3 and YL3 components could not be distinguished in SSPL, and therefore, we analyzed the width and intensity of the combined RY3 band at higher temperatures. Figures 6 and 7 show the temperature dependences of the full width at half maximum (FWHM) and normalized integrated PL intensity, respectively, of the RY3 band.

In the limit of low temperatures, the FWHM of the RY3 band in SSPL (~ 0.37 eV) is equal to that of the RL3 component, because the YL3 component is much weaker [Figs. 4(a) and 6]. With increasing temperature from 100 to 200 K, the FWHM of the combined RY3 band abruptly increases by almost 0.3 eV due to the fact that relative contributions of the RL3 and YL3 components in SSPL become nearly equal [Fig. 4(b)]. Between 200 and 600 K, no significant change in
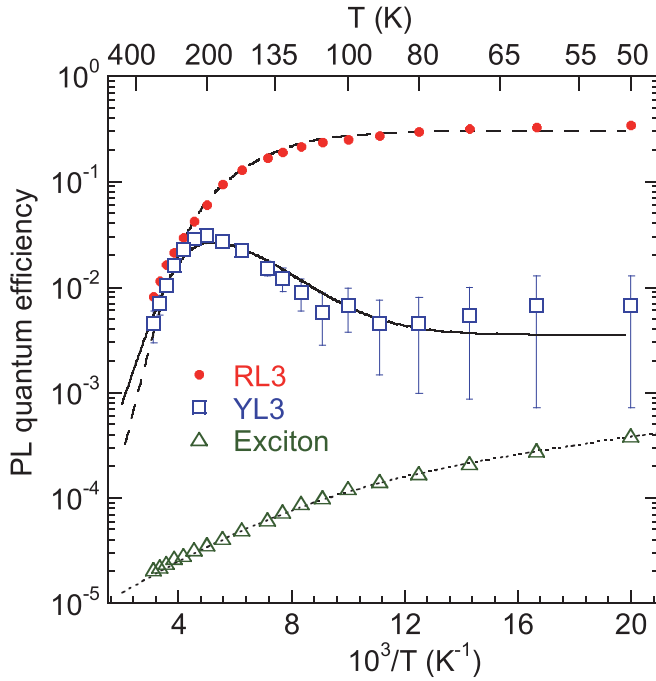
FIG. 5. Temperature dependence of the PL quantum efficiency for the RL3 and YL3 components of the RY3 band (sample H106, $P_{exc} = 10^{-4}$ W/cm^2). The lines are calculated using Eq. (1) with the following parameters: $\eta_{0i} = 0.3$ and $C_3 = 0$ for the RL3 component, $\eta_{0i} = 0.0035$ and $C_3 = 1100$ for the YL3 component; $C_1 = 100$, $C_2 = 2 \times 10^5$, $E_1 = 0.06$ eV, $E_2 = 0.22$ eV for both components; $\eta_{0i} = 0.004$, $C_1 = 60$, $C_2 = 600$, $C_3 = 0$, $E_1 = 8$ meV, and $E_2 = 35$ meV for the exciton band. The error bars for the YL3 component are large for temperatures between 50 and 100 K, because the YL3 component, with no visible ZPL, is covered by much stronger RL3 component. At $T < 50$ K, the YL3 ZPL can be resolved, so that uncertainty decreases: $\eta_{0,YL3} = 0.010 \pm 0.003$ at $T = 18$ K (not shown).

the FWHM of the RY3 band is observed. This may indicate that the ratio between the YL3 and RL3 intensities does not change above 200 K. However, below we show that an assumption that this ratio continues to increase above 200 K may also be valid. We fit the temperature dependence of FWHM, $W_i(T)$, for the RL3 and YL3 components (obtained from TRPL experiments) with the following expression obtained in the one-dimensional configuration-coordinate model [4]:

$$W_i(T) = W_i(0)\sqrt{\coth\left(\frac{\hbar\Omega_{0i}^e}{kT}\right)}, \qquad (2)$$

where $\hbar\Omega_{0i}^e$ is the effective phonon energy in the excited state of the defect. The obtained parameters $\hbar\Omega_{0i}^e$ (35 and 60 meV) are reasonable for defects in GaN [4]. The dependences were extrapolated into the region of high temperatures, where the TRPL data are unavailable (Fig. 6). By using these dependences, together with the experimentally obtained values of $W_i(0)$, the temperature dependence of the FWHM for the broad RY3 band was calculated (the solid curve in Fig. 6). In these calculations, the RL3 and YL3 components were simulated using Gaussian curves, with $W_i(T)$ found from Eq. (2), separated by 0.32 eV. The ratio of RL3 and YL3
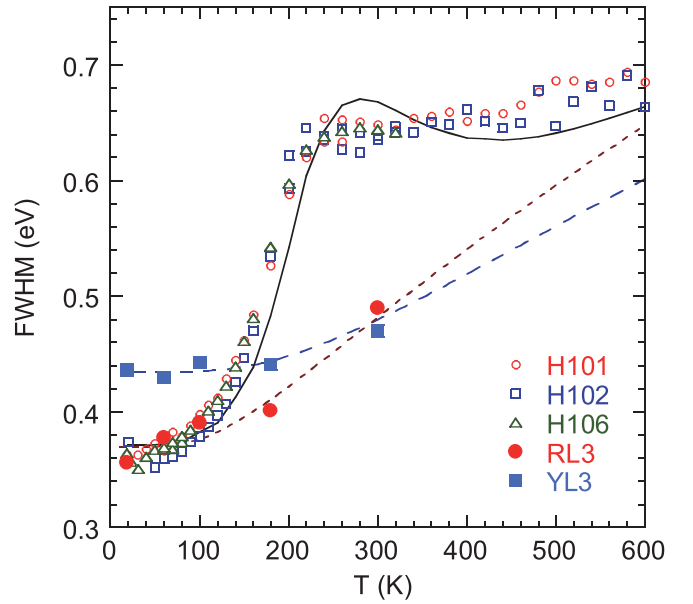

FIG. 6. Temperature dependence of the FWHM of the combined RY3 band and its components in samples with strong RY3 band. Empty symbols show the FWHM of the broad RY3 band in SSPL. Filled symbols show the FWHM of the RL3 and YL3 components obtained from TRPL. The dashed lines are calculated using Eq. (2) with the following parameters: $W_i(0) = 0.37$ eV and $\hbar\Omega_{0i}^e = 0.035$ eV for the RL3 component and $W_i(0) = 0.435$ eV and $\hbar\Omega_{0i}^e = 0.060$ eV for the YL3 component.

intensities, calculated using Eq. (1) with parameters given in the caption to Fig. 5, increases from 0.4 at $T = 200$ K to 4 at $T = 600$ K. The discrepancy between the predicted temperature dependence of the RY3 band (the solid line) and the actual experimental data in Fig. 6 can be attributed to significant assymetry of the RL3 and YL3 components and different energy shifts of these components with increasing temperature. The above analysis of the FWHM suggests that the ratio of the YL3 to RL3 components, which increases between 100 and 200 K, may continue to increase up to 600 K.

The PL intensity integrated over the entire RY3 band decreases with an activation energy of about 0.2 eV between 240 and 400 K (Fig. 7). At higher temperatures, the slope of the quenching increases, and the activation energy of this process is estimated as ~0.5 eV. The RL3 and YL3 components remain indistinguishable above 300 K (the inset in Fig. 7). There may be at least two explanations for the RY3 quenching at $T > 200$ K [18].

First, when PL quenching is caused by thermal emission of holes from a defect level to the valence band (the Schön-Klasens mechanism), the $\eta_i(T)$ dependence is described with the following expression [18,19]:

$$\eta_i(T) = \eta_{0i}\left[1 + \frac{(1 - \eta_{0i})\tau_{0i}^{PL}}{\tau_i^{th}}\right]^{-1}, \qquad (3)$$

where τ_{0i}^{PL} is the "waiting time" for a bound hole before electron-hole recombination occurs (usually, the PL lifetime), and τ_i^{th} is the characteristic time of the thermal emission of
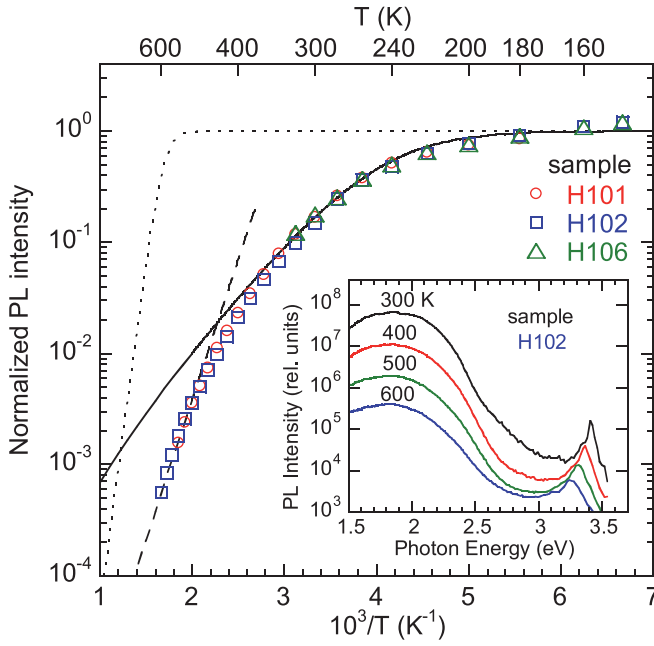
FIG. 7. Temperature dependences of the integrated SSPL intensity (RL3 + YL3) in samples with strong RY3 band. All dependences are normalized at $T = 170$ K for convenience of comparison. The solid line is calculated using Eq. (A17) in the Appendix with the following parameters: $C_1 = 100$, $E_1 = 0.06$ eV, $C_2 = 0.75 \times 10^{-14} N_v$ (where $N_v = 3.2 \times 10^{15} T^{3/2}$), and $E_2 = 0.2$ eV. The dashed line shows the calculated dependence $3.5 \times 10^{-8} \exp(-E_3/kT)$ with $E_3 = 0.5$ eV. The dotted line is calculated using Eqs. (3) and (4) with $\eta_{0i} = 0.3$, $C_{pi} = 10^{-6}$ cm^3/s, $E_i = 1.13$ eV, and $\tau_{0i}^{PL} = 200 \, \mu$s.

holes from this level to the valence band:

$$\tau_i^{th} = \frac{g \exp\left(\frac{E_i}{kT}\right)}{C_{pi} N_v}. \quad (4)$$

Here, C_{pi} is the hole-capture coefficient for the ith defect, E_i is the defect ionization energy, g is the degeneracy of the defect level (assumed to be 2), and N_v is the effective density of states in the valence band.

In another mechanism of PL quenching (the Seitz-Mott mechanism), a defect becomes a nonradiative recombination center above certain temperature due to overcoming a barrier between adiabatic potentials of the excited and ground states of the defect. In this case,

$$\tau_i^{th} = \nu^{-1} \exp\left(\frac{E_i^*}{kT}\right), \quad (5)$$

where ν is the vibrational frequency of the defect (about 10^{13} s^{-1}) and E_i^* is the barrier height.

For majority of defects in undoped GaN (the UVL, BL1, YL1, and RL1 bands), the PL is quenched due to the Schön-Klasens mechanism, and τ_{0i}^{PL} in Eq. (3) is the PL lifetime at temperatures before thermal quenching. For transitions from the conduction band in n-type semiconductors,

$$\tau_{0i}^{PL} = \frac{1}{C_{ni} n}, \quad (6)$$

where n is the concentration of free electrons and C_{ni} is the electron-capture coefficient for the ith defect [9]. While

Eq. (3) is valid for description of thermal quenching of both RL3 and YL3 components, parameter τ_{0i}^{PL} for the YL3 component is several orders of magnitude smaller than the measured YL3 lifetime, which will be explained below.

According to the model shown in Fig. 1, the thermal quenching of both the RL3 and YL3 components occurs *simultaneously* due to competition between the thermal emission of holes from the A_3 level to the valence band with the characteristic time τ_{A3}^{th} and the "waiting time" of the holes at this level, τ^*, before they recombine with electrons. Since the transitions of holes from level A_3 to levels A_1 and A_2 occur in parallel (transitions 3 and 2 in Fig. 1), τ^* can be found from the following expression (see Appendix):

$$\frac{1}{\tau^*} = \frac{1}{\tau_{31}} + \frac{1}{\tau_{32}}. \quad (7)$$

Note that the RL3 lifetime, which is *measured* in TRPL experiments at temperatures before the thermal quenching, $\tau_{0,RL3}$, is equal to τ^*, because the RL3 decay (transition from A_3 to A_1) is shunted by the escape of holes from A_3 to A_2. Thus the temperature dependences of both the RL3 and YL3 components in SSPL can be described with Eq. (3), in which $\tau_{0i}^{PL} = \tau_{0,RL3} = \tau^* \approx 10$ ns.

From the fit to the experimental data between 160 and 400 K (Fig. 7) with Eqs. (3) and (4), we find that $E_i = 0.15$ eV and $(1 - \eta_{0i}) C_{pi} \tau_{0i}^{PL} = 2 \times 10^{-16}$ cm^3. The fit with Eq. (A17) from Appendix provides a very similar dependence, yet with slightly different parameters: $E_i = 0.2$ eV and $(1 - \eta_{0i}) C_{pi} \tau_{0i}^{PL} = 1.5 \times 10^{-14}$ cm^3. With $\tau_{0i}^{PL} \approx 10^{-8}$ s for the A_3 state, we obtain $C_{pi} = 10^{-8} - 10^{-6}$ cm^3/s, which is a reasonable value for the hole-capture coefficient. Thermal emission of holes from the A_2 level to the valence band with the characteristic time τ_{A2}^{th} can be completely ignored at $T < 400$ K. Indeed, the quenching of the YL3 component due to this reason is expected to begin only at $T > 600$ K for reasonable parameters of this state ($E_i = 1.13$ eV, $\tau_{0i}^{PL} \approx 200 \, \mu$s and $C_{pi} \approx 10^{-8} - 10^{-6}$ cm^3/s), see the dotted line in Fig. 7.

In the second model (the Seitz-Mott mechanism), a very similar dependence (indistinguishable from the solid line in Fig. 7) can be obtained by using Eqs. (3) and (5) with $E_i^* \approx 0.2$ eV and $\nu \tau_{0i}^{PL} \approx 10^4$. Although these parameters are also reasonable (e.g., $\nu \approx 10^{13} - 10^{12}$ s^{-1} and $\tau_{0i}^{PL} \approx 10^{-9} - 10^8$ s), the Seitz-Mott mechanism of PL quenching seems unlikely in this case. Indeed, with such a small barrier between adiabatic potentials of the excited and ground states, a PL band width is expected to increase dramatically at temperatures when PL quenching is observed. However, the temperature variation the RY3 band width is insignificant between 200 and 600 K, and the broadening of its RL3 and YL3 components with temperature is not abnormal (Fig. 6).

C. Temperature dependence of PL lifetime

Recombination of electrons and holes via the RY3 center, according to the model shown in Fig. 1, involves several characteristic times that will be defined here. In TRPL experiments, PL intensity may decay exponentially after a laser pulse, as $\exp(-t/\tau^{PL})$, where τ^{PL} is PL lifetime ($\tau^{PL} \equiv \tau_{RL3}$ for the RL3 and $\tau^{PL} \equiv \tau_{YL3}$ for the YL3). The characteristic
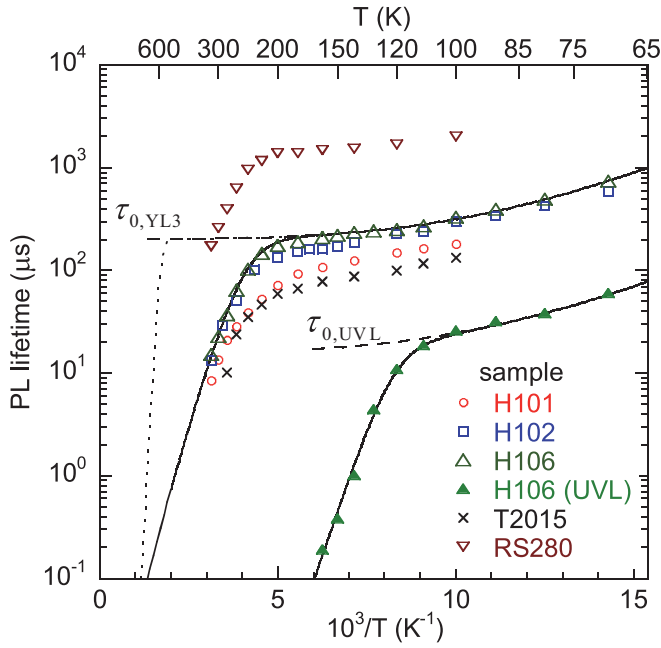
FIG. 8. Temperature dependence of PL lifetime of the YL3 component in samples with strong RY3 band. $P_0 = 5 \times 10^{21}$ cm^{-2} s^{-1}. The dependence for the UVL band in sample H106 is shown for comparison. The dashed lines for τ_{0i}^{PL} in sample H106 are calculated using Eq. (6) with $C_{ni} = 2.5 \times 10^{-13}$ cm^3/s for the YL3 component and $C_{ni} = 3.2 \times 10^{-12}$ cm^3/s for the UVL band, where the $n(T)$ dependence is calculated using Eq. (8) with $N_D = 7.0 \times 10^{16}$ cm^{-3}, $N_A = 4.3 \times 10^{16}$ cm^{-3}, and $E_D = 15$ meV. The solid lines are calculated using Eqs. (9) and (4) with the following parameters: $(1 - \eta_{0i})C_{pi}\tau_{0i}^{PL} = 1 \times 10^{-15}$ cm^3 and $E_i = 0.18$ eV for the YL3 component; $C_{pi} = 1 \times 10^{-6}$ cm^3/s and $E_i = 0.182$ eV for the UVL band. The dotted line for the YL3 component is calculated using the same equations with $C_{pi} = 10^{-6}$ cm^3/s, $E_i = 1.13$ eV, and $\tau_{0i}^{PL} = 200\,\mu$s.

times for transitions 1, 2, 3, 4, 5, 6, 7 and 8 in Fig. 1 are defined as τ_{p3}, τ_{32}, τ_{31}, τ_{n2}, τ_{n1}, τ^{th}, τ_{nS}, and τ_{pS}, respectively. Note that the measured RL3 lifetime, τ_{RL3}, is approximately equal to τ_{31} only at $T < 100$ K. At higher temperatures, competing transitions 2 and 6 reduce it to τ^* [Eq. (7)] and eventually to $\tau_{RL3} = (1/\tau_{31} + 1/\tau_{32} + 1/\tau_{A3}^{th})^{-1}$. Similarly, τ_{YL3} is not always equal to τ_{n2}.

The electron transitions causing the YL3 emission are reliably established thanks to the observation of its ZPL and phonon-related fine structure [11]. At $T < 50$ K, the decay of the YL3 component after a laser pulse is nonexponential, indicating that this component is produced by transitions from shallow donors to a deep acceptor with the transition level located at 1.13 eV above the valence band. At $T > 50$ K, the donor-acceptor-pair (DAP)-type transitions are replaced with transitions from the conduction band to the same acceptor (eA transitions). The decay of the YL3 intensity after a laser pulse becomes nearly exponential, so that effective PL lifetime can be determined [20]. Figure 8 shows the temperature dependence of the YL3 lifetime for several GaN samples with different n. Below, we analyze a region with weak $\tau^{PL}(T)$ dependence ($T = 50 - 200$ K) and a region where τ^{PL} decreases exponentially with temperature ($T > 200$ K).

At 50 K $< T < 200$ K, $\tau_{YL3} = \tau_{0,YL3}$, and the YL3 life-time slowly decreases with increasing temperature due to increasing n. To find the $n(T)$ dependence for a particular sample, we first fit the $\tau_{0i}^{PL}(T)$ dependence for the UVL band with Eq. (6) (an example for sample H106 is shown in Fig. 8). Since parameter C_{ni} for the UVL band is reliably established, $(3.2 \pm 0.3) \times 10^{-12}$ cm^3/s [9], the $n(T)$ dependence can be found from the $\tau_{0,UVL}(T)$ dependence. This dependence was simulated with the following expression:

$$\frac{n(n + N_A)}{N_D - N_A - n} = \frac{N_c}{g} \exp\left(-\frac{E_D}{kT}\right), \tag{8}$$

where the concentrations of shallow donors (N_D), all acceptors (N_A), and effective ionization energy for shallow donors (E_D) were selected to match the temperature dependence of $\tau_{0,UVL}$ at $T < 100$ K. In the same way, the $n(T)$ dependence was determined for other samples. In particular, $n(100$ K$)$ is 3×10^{15} and 5×10^{16} cm^{-3} for samples RS280 and T2015, respectively, and it is close to 1×10^{16} cm^{-3} for other samples analyzed in Fig. 8. All these values roughly agree with the data obtained from temperature-dependent Hall-effect measurements.

Next, the simulated $n(T)$ dependence was used to fit the experimental data for the YL3 component with Eq. (6) (Fig. 8). The electron-capture coefficient for the YL3 component, determined from this fit for sample H106 at $T < 200$ K ($C_{n,YL3} = 2.5 \times 10^{-13}$ cm^3/s), is close to the value previously found from the analysis of several GaN samples [$C_{n,YL3} = (2.0 \pm 0.5) \times 10^{-13}$ cm^3/s)] [9]. The presented evidence strongly supports the attribution of the YL3 component with the ZPL at 2.38 eV at $T > 50$ K to transitions from the conduction band to the A$_2$ level located at 1.13 eV above the valence band.

The behavior of the YL3 lifetime at temperatures above 200 K (exponential decrease with $E_i \approx 0.2$ eV, similar to PL intensity behavior) is puzzling. At first glance, a simple model of a defect with one energy level, predicts the following $\tau_i^{PL}(T)$ dependence for defects in an n-type semiconductor [9,20]:

$$\tau_i^{PL}(T) = \tau_{0i}^{PL}\left[1 + \frac{(1 - \eta_{0i})\tau_{0i}^{PL}}{\tau_i^{th}}\right]^{-1}, \tag{9}$$

which looks very similar to Eq. (3) for the PL intensity dependence. However, in the proposed model of the RY3 center, parameter τ_{0i}^{PL} in Eq. (9) is the "waiting time" at the A$_2$ level ($\tau_{0i}^{PL} = \tau_{0,YL3} \approx 200\,\mu$s at $T > 120$ K), while that in Eq. (3) is the "waiting time" at the A$_3$ level ($\tau_{0i}^{PL} = \tau^* \approx 10$ ns), see Appendix. The exponential decrease of τ_{YL3} is expected to begin at a temperature when the characteristic time of thermal emission of holes from the A$_2$ level (τ_{A2}^{th}) becomes equal to the "waiting time" of holes at this level ($\tau_{0,YL3}$), i.e., at $T > 600$ K (the dotted line in Fig. 8). Instead, the decrease of τ_{YL3} begins at 200 K.

In principle, such exponential decrease of τ_{YL3} at $T > 200$ K could be caused by thermal emission of holes from the A$_2$ level to a level located at ~0.2 eV below it. The A$_3$ level is located significantly farther from A$_2$, so that another excited state, closer to A$_2$, would have to be introduced. At this time, we find it unnecessary to complicate the relatively simple
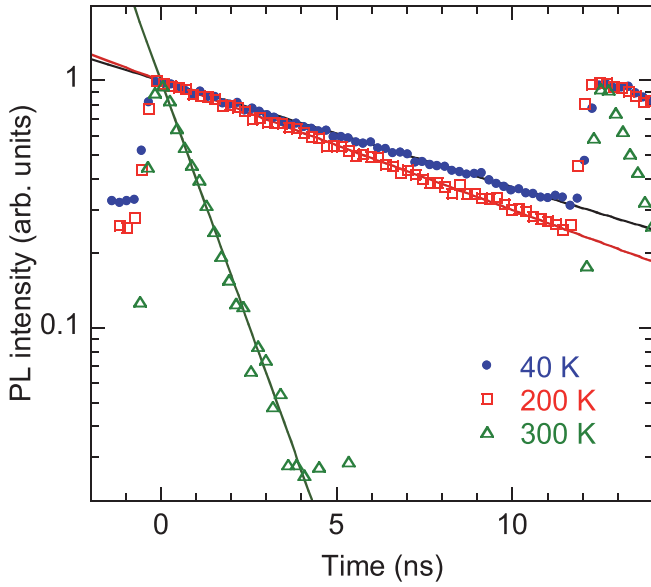
FIG. 9. Transients of the RL3 emission (between 1.78 and 1.86 eV) for sample H102 at selected temperatures obtained by using a frequency-tripled femtosecond pulsed Ti-sapphire laser (266 nm, 25 W/cm^2, 80 MHz). Every fifth point is shown. The dependences are fitted using the following expression: $I^{\mathrm{PL}}(t) = \exp(-t/\tau^{\mathrm{PL}})$, with $\tau^{\mathrm{PL}} = 10.1$ ns (40 K), 8.3 ns (200 K), and 1.1 ns (300 K).

model, which explains vast majority of experimental data. Identification of the RY3 center and analysis of its electronic structure by using first-principles calculations may help to resolve the puzzle.

Next, we discuss the PL lifetime of the RL3 component. The decay of the RL3 emission after a laser pulse is exponential, even at $T = 18$ K. The PL lifetime is nearly independent of temperature up to 200 K (Fig. 9), and about the same in different samples ($\tau_{0i}^{\mathrm{PL}} \equiv \tau_{0,\mathrm{RL3}} \approx 8 - 10$ ns). This is typical for internal transitions, where the PL lifetime is independent of the concentration of free electrons. At higher temperatures, the τ_{RL3} decreases with the activation energy of 0.18 eV (Fig. 10). A similar trend for the τ_{RL3} was observed in TRPL excited with a nitrogen laser, yet the activation energy could not be reliably determined in these experiments because of poor temporal resolution. This decrease in τ_{RL3} is explained by the thermal emission of holes from the excited state A_3 to the valence band. The dependence in Fig. 10 is fitted using Eq. (9) with $\tau_{0,\mathrm{RL3}} = 10$ ns, $E_i = 0.17$ eV, and $C_{pi} = 1 \times 10^{-7}$ cm^3/s. A similar fit (the dashed line in Fig. 10) was obtained by accounting for the temperature dependence of $\tau_{0,\mathrm{RL3}} = \tau^*$, in agreement with the model shown in Fig. 1. In this case, $E_i = 0.22$ eV and $C_{pi} = 2 \times 10^{-7}$ cm^3/s.

We conclude that the thermal quenching of the RL3 and YL3 components, as well as the temperature dependence of the RL3 lifetime can be attributed to thermal emission of holes from the A_3 level located at about 0.2 eV above the valence band. The temperature dependences of the RY3 band and its components, including the rise of the YL3 intensity simultaneously with the quenching of the RL3 component, were reliably reproduced in other samples. The identical interplay of the two components in various samples provides
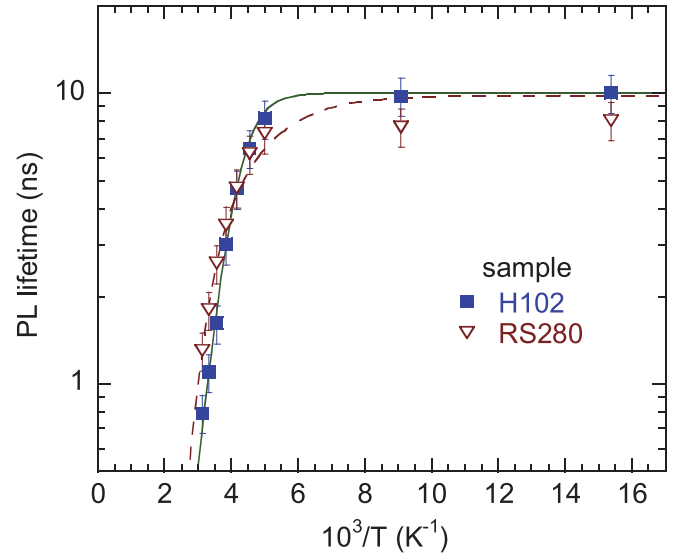

FIG. 10. Temperature dependences of the RL3 emission lifetime in samples H102 and RS280 obtained from TRPL excited with a frequency-tripled femtosecond pulsed Ti-sapphire laser. The solid line is calculated using Eqs. (9) and (4) with the following parameters: $\tau_0^{\mathrm{PL}} \equiv \tau_{0,\mathrm{RL3}} = 10$ ns, $\eta_{0i} = 0.3$, $C_{pi} = 1 \times 10^{-7}$ cm^3/s, and $E_i = 0.17$ eV. The dashed curve accounts for the temperature dependence of $\tau_{0,\mathrm{RL3}}$ (see the Appendix) and is calculated with the following parameters: $\eta_{0i} = 0.3$, $C_{pi} = 2 \times 10^{-7}$ cm^3/s, $E_i = 0.22$ eV, $\tau_{31} = 10$ ns, $\tau_{32} = [2 \times 10^6 + 3 \times 10^9 \exp(-\Delta E/kT)]^{-1}$, where $\Delta E = 0.07$ eV.

a strong argument that they are related to the same defect, the RY3 center. Further insight into the unusual properties of the RY3 center can be obtained from the analysis of the excitation intensity dependences.

D. Dependence of PL intensity on excitation intensity in SSPL

Excitation-dependent PL measurements can be used to determine the concentration of defects involved in PL, as well as to resolve overlapped PL bands from different defects [15]. At $T > 50$ K, the YL3 component is caused by transitions of electrons from the conduction band to the acceptor level located at 1.13 eV above the valence band. For such transitions, the concentration of related defects can be determined from the dependence of the PL intensity on the excitation intensity when the PL quantum efficiency and PL lifetime are known [15,21]. The dependences of the SSPL quantum efficiency on excitation intensity for the RL3 and YL3 components at $T = 80$ and 180 K are shown in Fig. 11.

At $T = 180$ K, the saturation of the RL3 and YL3 intensities begins at $P_{\mathrm{exc}} \approx 10^{-2}$ W/cm^2 [Fig. 11(b)]. At $T = 80$ K, the YL3 component is too weak to be reliably resolved from the more intense RL3 component, so the beginning of its saturation at $P_{\mathrm{exc}} \approx 10^{-2} - 10^{-1}$ W/cm^2 cannot be determined reliably [Fig. 11(a)]. The excitation intensity dependence for defect-related PL bands can be fitted with the following expression [15,21]:

$$\eta_i(P_0) = \eta_{0i} \frac{P_i^{\mathrm{cr}}}{P_0} \ln\left(1 + \frac{P_0}{P_i^{\mathrm{cr}}}\right) \tag{10}$$
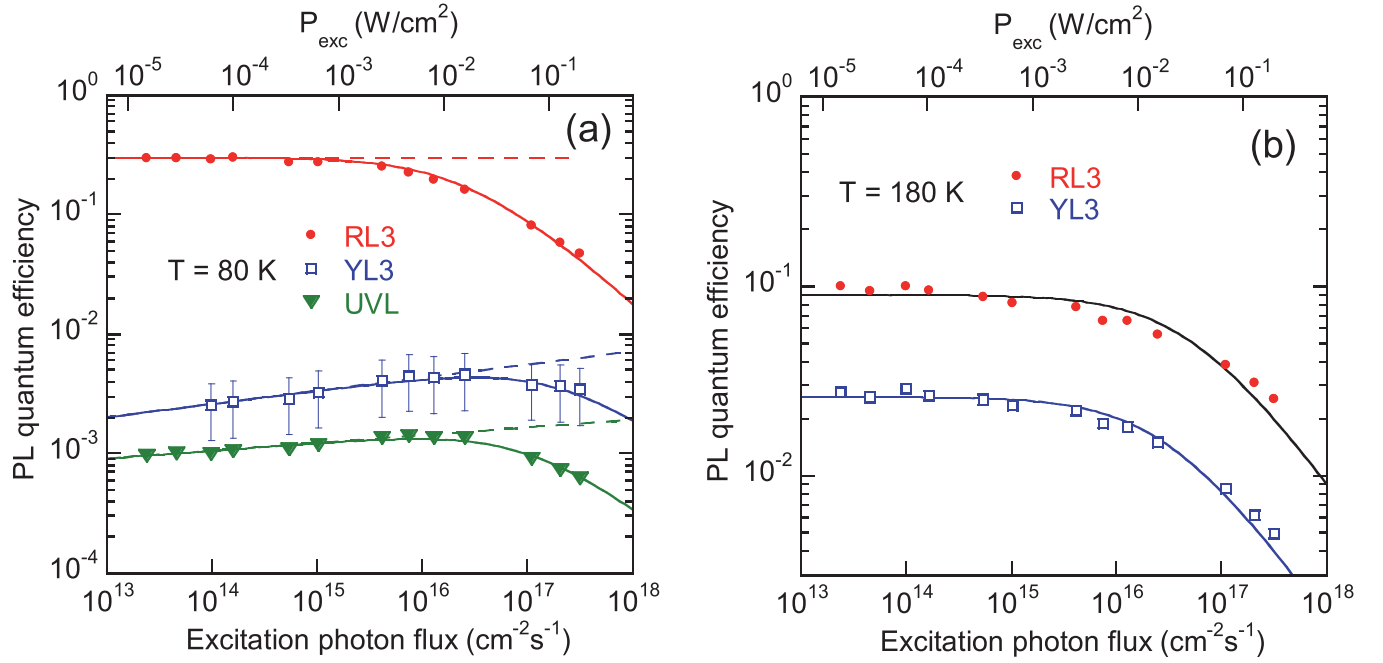
FIG. 11. Dependence of the PL quantum efficiency of the RL3, YL3 and UVL bands in sample H106. (a) $T = 80$ K. The lines are calculated using Eqs. (10) and (11) with the following parameters: $N_i = 3 \times 10^{16}$ cm^{-3}, $\tau_i^{\lim} = 5 \times 10^{-4}$ s, and $\eta_0 = 0.00008(P_0)^{0.11}$ (YL3); $N_i/\tau_i^{\lim} = 5 \times 10^{20}$ cm^{-3} s^{-1}, and $\eta_{0i} = 0.3$ (RL3); $N_i = 2.8 \times 10^{14}$ cm^{-3}, $\tau_i^{\lim} = 4 \times 10^{-5}$ s, and $\eta_{0i} = 0.00013(P_0)^{0.065}$ (UVL). The dashed lines for the YL3 and UVL bands show simulated η_{0i} values that account for a weak dependence on excitation intensity not related to PL saturation. (b) $T = 180$ K. The lines are calculated using Eqs. (10) and (11) with the following parameters: $N_i = 1.0 \times 10^{16}$ cm^{-3}, $\tau_i^{\lim} = 2 \times 10^{-4}$ s, and $\eta_{0i} = 0.026$ (YL3); $N_i/\tau_i^{\lim} = 3 \times 10^{20}$ cm^{-3} s^{-1}, and $\eta_{0i} = 0.09$ (RL3); $\alpha = 1.2 \times 10^5$ cm^{-1}.

with

$$P_i^{\mathrm{cr}} = \frac{N_i}{\eta_{0i}\alpha\tau_i^{\lim}}. \qquad (11)$$

Here, N_i is the concentration of the related defect, $\tau_i^{\lim}$ is the longest time in the recombination process (usually, $\tau_i^{\lim} = \tau_{0i}^{\mathrm{PL}}$), η_{0i} is the quantum efficiency in the limit of low excitation intensity, and α is the absorption coefficient ($\alpha \approx 1.2 \times 10^5$ cm^{-1} for GaN at $\hbar\omega = 3.815$ eV for a HeCd laser) [22]. According to Eq. (10), the saturation of PL begins at $P_0 \approx P_i^{\mathrm{cr}}$, where low value of P_i^{cr} corresponds to a low concentration of defects, high quantum efficiency, and long PL lifetime.

For transitions from the conduction band to a defect level, the fit of the experimental data with Eqs. (10) and (11) includes only one fitting parameter, N_i, because τ_{0i}^{PL} can be directly determined from TRPL, and η_{0i} can be estimated from the temperature dependence of SSPL or by comparison with calibrated GaN samples [15–17]. This approach is valid for the YL3 and UVL bands, since both these bands are caused by transitions from the conduction band at $T > 50$ K, and their PL lifetimes are known (Fig. 8). Due to the large uncertainty of the YL3 component contribution at $T = 80$ K [shown with large error bars in Fig. 11(a)], the more reliable data at $T = 180$ K [Fig. 11(b)] are taken for this band for the quantitative analysis. With $\eta_{0i} = 0.026$ and $\tau_i^{\lim} = \tau_{0,\mathrm{YL3}} = 2 \times 10^{-4}$ s for the YL3 band at $T = 180$ K, and $\eta_{0i} = 0.001$ and $\tau_i^{\lim} = \tau_{0,\mathrm{UVL}} = 4 \times 10^{-5}$ s for the UVL band at $T = 80$ K, we obtain $N_{\mathrm{YL3}} = 1.0 \times 10^{16}$ cm^{-3}

and $N_{\mathrm{UVL}} = 2.8 \times 10^{14}$ cm^{-3} for the YL3 and UVL bands, respectively.

As for the RL3 component, the fit using Eq. (10) with $\eta_{0i} = 0.3$ and $\tau_i^{\lim} = \tau_{0,\mathrm{RL3}} = 10$ ns at $T = 80$ K would lead to $N_{\mathrm{RL3}} = 5 \times 10^{12}$ cm^{-3}, an unreasonably small value for a PL band with such high quantum efficiency. A very low N_i value for a PL band with a very high η_{0i} would indicate a very large C_{pi}. Indeed, the PL quantum efficiency for the ith defect, with a concentration N_i, in an n-type semiconductor is $\eta_{0i} = C_{pi}N_ip/G$ [16]. If we use Eq. (10) to find the concentrations N_i and N_j for two defects, and we know the hole-capture coefficient for one of them, we can find C_{pi} for the other defect from the following relationship:

$$\frac{C_{pj}}{C_{pi}} = \frac{\eta_{0j}N_i}{\eta_{0i}N_j}, \qquad (12)$$

where the ratio η_{0j}/η_{0i} is equal to the ratio of the integrated intensities of the related PL bands. The C_{pi} for the RL3 component can be estimated by comparing it to the much weaker UVL band [Fig. 11(a)], for which $C_{p,\mathrm{UVL}} = 1 \times 10^{-6}$ cm^3/s [4,15]. Other parameters are found from fitting the experimental data with Eq. (10): $\eta_{0,\mathrm{UVL}} = 1 \times 10^{-3}$ and $N_{\mathrm{UVL}} = 2.8 \times 10^{14}$ cm^{-3}. With $\eta_{0,\mathrm{RL3}} = 0.3$ and $N_{\mathrm{RL3}} = 5 \times 10^{12}$ cm^{-3} for the RL3 band, we find $C_{p,\mathrm{RL3}} \approx 0.02$ cm^3/s from Eq. (12); this is an unreasonably large value. Note that the hole-capture coefficient can be presented as the product of the hole-capture cross-section, σ_{pi}, and the mean thermal velocity, $\langle v_p \rangle$, of holes in the valence band [23]. With $\langle v_p \rangle \approx 10^7$ cm/s at 80 K, the $C_{p,\mathrm{RL3}}$ coefficient converts to

$\sigma_{p,\mathrm{RL3}} \approx 2 \times 10^{-9}\,\mathrm{cm}^2$. This is much larger than any other known hole-capture cross-section for defects in semiconductors. The largest hole-capture cross-sections were reported for giant traps in Si and Ge : $\sigma_{pi} \approx 10^{-11}\,\mathrm{cm}^2$ at $T = 4$ K, and $\sigma_{pi} \approx 10^{-13}\,\mathrm{cm}^2$ at $T = 80$ K. [23] Thus there must be another explanation for the high quantum efficiency of the RL3 component, its early saturation with increasing excitation intensity in SSPL, and very short lifetime, which is proposed below.

On the other hand, if we assume that the RL3 component is caused by the same defect as the YL3 component, with a concentration of $N_{\mathrm{RY3}} = 1.0 \times 10^{16}\,\mathrm{cm}^{-3}$, we would obtain from Eq. (12) a reasonable value of the hole capture coefficient: $C_{p,\mathrm{RL3}} \approx 10^{-5}\,\mathrm{cm}^3/\mathrm{s}$. However, in this case, by fitting the $\eta_i(P_0)$ dependence with Eq. (10), we discover that $\tau_i^{\mathrm{lim}} \approx 20\,\mu\mathrm{s}$ at $T = 80$ K and $30\,\mu\mathrm{s}$ at $T = 180$ K. This time cannot be the PL lifetime (which is ~ 10 ns for the RL3 band), but is actually the characteristic time of the slowest transition in a multistep electron-hole recombination, where one of the steps is the fast radiative transition which causes the RL3 emission. According to the model presented in Fig. 1, the only step which could be slow is transition 5, i.e., $\tau_{n1} = 20 - 30\,\mu\mathrm{s}$, since transitions 1 and 3 are determined to be significantly faster (see Appendix). Finally, from Eq. (12), we obtain $C_{p,\mathrm{RL3}} = 8.4 \times 10^{-6}\,\mathrm{cm}^3/\mathrm{s}$ and $C_{p,\mathrm{YL3}} = 1.2 \times 10^{-7}\,\mathrm{cm}^3/\mathrm{s}$ at $T = 80$ K, and $C_{p,\mathrm{RL3}} = 2.5 \times 10^{-6}\,\mathrm{cm}^3/\mathrm{s}$ and $C_{p,\mathrm{YL3}} = 9 \times 10^{-7}\,\mathrm{cm}^3/\mathrm{s}$ at $T = 180$ K. Note that the concentration of the defect responsible for the RY3 center is fixed ($1 \times 10^{16}\,\mathrm{cm}^{-3}$) in these estimates, and the quantum efficiencies of the RL3 and YL3 components change with temperature proportionally to the changes in the coefficients C_{pi}. The sum of the capture coefficients is equal to the hole-capture coefficient for the excited delocalized state (0.2 eV): $C_{p3} = C_{p,\mathrm{RL3}} + C_{p,\mathrm{YL3}} = 8.5 \times 10^{-6}\,\mathrm{cm}^3/\mathrm{s}$ at $T = 80$ K and $3.4 \times 10^{-6}\,\mathrm{cm}^3/\mathrm{s}$ at $T = 180$ K. As the temperature increases from 18 to 200 K (before the RY3 band quenches), the integrated intensity of the RY3 band decreases by a factor of 2–3 due to the decrease in the C_{p3}. Similar results were obtained for other samples.

In particular, the RY3 band is relatively intense in sample RS280, but its saturation with excitation intensity occurs at much lower excitation intensities (Fig. 12). This may indicate that the concentration of the RY3 centers in sample RS280 is much lower than that in sample H106. For sample RS280, by using Eq. (10) with the PL lifetime values obtained from TRPL, we have found the concentrations of the $\mathrm{Mg_{Ga}}$ and $\mathrm{Zn_{Ga}}$ defects responsible for the UVL and BL1 bands ($N_{\mathrm{UVL}} = 3 \times 10^{14}\,\mathrm{cm}^{-3}$ and $N_{\mathrm{BL1}} = 2.8 \times 10^{15}\,\mathrm{cm}^{-3}$, respectively), and the $N_i/\tau_i^{\mathrm{lim}}$ ratio for the RL3 component ($3.2 \times 10^{18}\,\mathrm{cm}^{-3}\,\mathrm{s}^{-1}$). The concentration of the RY3 defect is $N_{\mathrm{RY3}} \approx 2.2 \times 10^{14}\,\mathrm{cm}^{-3}$, which is found from Eq. (12) with the previously calculated value $C_{p3} = 8 \times 10^{-6}\,\mathrm{cm}^3/\mathrm{s}$ at $T = 80$ K. Alternatively, from the BL1 band intensity dependence on excitation intensity (for which $C_{p,\mathrm{BL1}} = 4.9 \times 10^{-7}\,\mathrm{cm}^3/\mathrm{s}$) [7], we find that $N_{\mathrm{RY3}} \approx 1.4 \times 10^{14}\,\mathrm{cm}^{-3}$. Based on the data for the UVL and BL1 bands in sample RS280 and accounting for the $N_i/\tau_i^{\mathrm{lim}}$ ratio for the RL3 component found from the fit with Eq. (10), we estimate that $N_{\mathrm{RY3}} \approx 2 \times 10^{14}\,\mathrm{cm}^{-3}$ (two orders of magnitude lower than in sample H106) and $\tau_{n1} \approx 60\,\mu\mathrm{s}$.

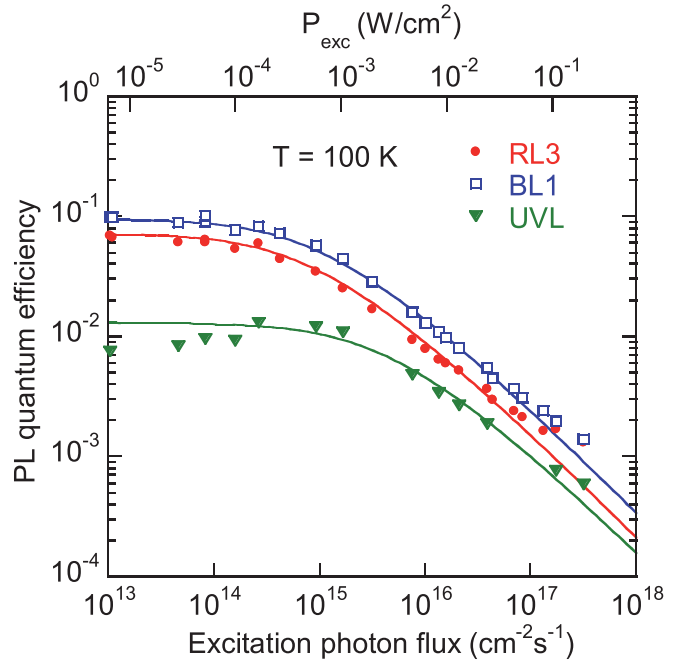

FIG. 12. Dependence of the PL quantum efficiency for the RL3, BL1, and UVL bands in sample RS280 at $T = 100$ K. The lines are calculated using Eq. (10) with the following parameters: $N_i/\tau_i^{\mathrm{lim}} = 3.2 \times 10^{18}\,\mathrm{cm}^{-3}\,\mathrm{s}^{-1}$, and $\eta_{0i} = 0.075$ (RL3); $N_i = 2.8 \times 10^{15}\,\mathrm{cm}^{-3}$, $\tau_i^{\mathrm{lim}} = t_i^{\mathrm{PL}} = 5.3 \times 10^{-3}$ s, and $\eta_{0i} = 0.095$ (BL1); $N_i = 3 \times 10^{14}\,\mathrm{cm}^{-3}$, $\tau_i^{\mathrm{lim}} = t_i^{\mathrm{PL}} = 1 \times 10^{-4}$ s, and $\eta_{0i} = 0.013$ (UVL); and $\alpha = 1.2 \times 10^5\,\mathrm{cm}^{-1}$.

By repeating this analysis for sample T2015, where the RY3 and BL1 bands are relatively intense (Fig. 2), we find $N_{\mathrm{BL1}} = 7 \times 10^{15}\,\mathrm{cm}^{-3}$ and $\tau_i^{\mathrm{lim}} = \tau_{0,\mathrm{BL1}} = 14\,\mu\mathrm{s}$ for the BL1 band at $T = 190$ K. Then, by taking $C_{p3} = 3 \times 10^{-6}\,\mathrm{cm}^3/\mathrm{s}$ for this temperature, we find $N_{\mathrm{RY3}} = 5 \times 10^{14}\,\mathrm{cm}^{-3}$ and $\tau_{n1} = 20\,\mu\mathrm{s}$ for the RY3 defect at $T = 190$ K. Thus, from independent experiments for several samples, we consistently obtain $\tau_{n1} = 20 - 60\,\mu\mathrm{s}$. This time characterizes the slowest of the processes in the electron-hole recombination, one of which is the fast (~ 10 ns) RL3 emission. Note that the concentrations of free electrons at $T = 100$ K, as follows from the PL lifetimes of the UVL, BL1, and GL1 bands, vary in wide range: $n = 3 \times 10^{15}$, 1.2×10^{16}, and $5 \times 10^{16}\,\mathrm{cm}^{-3}$ for samples RS280, H106, and T2015, respectively.

It appears that the hole-capture coefficient C_{p3} for the delocalized 0.2 eV state decreases with increasing temperature, which follows from the temperature dependence of the integrated RY3 intensity at temperatures below its quenching ($T < 200$ K) and from comparison with other PL bands by using Eq. (12). The C_{p3} decreases from about 10^{-5} to about $3 \times 10^{-6}\,\mathrm{cm}^3/\mathrm{s}$ as the temperature is increased from 18 to 180 K. One possible explanation is that, as in the case of giant traps in Si and Ge, [23] there is a ladder of excited states, not just a single effective-mass level. The $C_{p3}(T)$ dependence may also explain why from the temperature dependences of the RL3 and YL3 intensity (Sec. III B) and that of the RL3 lifetime (Sec. III C), we obtained $C_{p3} = 10^{-7} - 10^{-6}\,\mathrm{cm}^3/\mathrm{s}$ for the hole-capture by the excited state A_3 at temperatures between 200 and 300 K, which is lower than the values
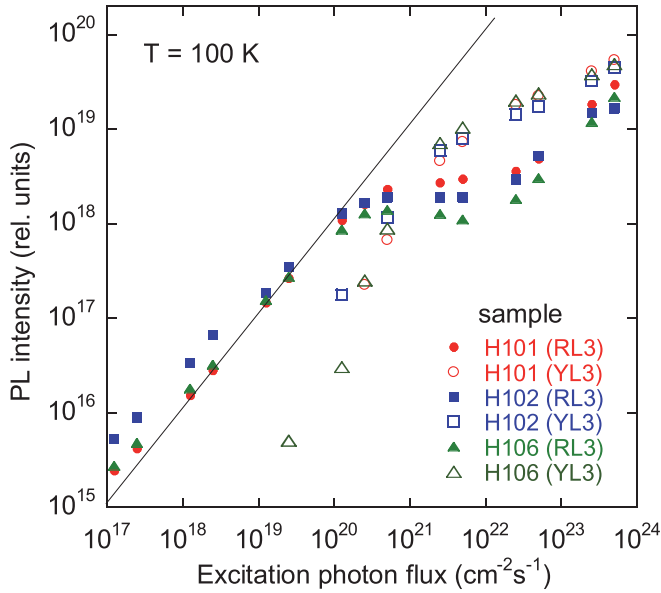
FIG. 13. Time-integrated PL intensity as a function of the excitation photon flux for the RL3 and YL3 components in three GaN samples at $T = 100$ K. A linear dependence (solid line) is shown as a guide to eye.

obtained from the excitation intensity dependences at $T = 80$ and 180 K (8×10^{-6} and 3×10^{-6} cm^3/s, respectively).

E. Dependence of PL intensity on excitation intensity in TRPL

Figure 13 shows the dependences of TRPL intensity on the excitation intensity at $T = 100$ K for the RL3 and YL3 components in three GaN samples with the strongest RY3 band. The PL intensity after a laser pulse is integrated over time for both components. In spite of the fact that the peak intensity is several orders of magnitude higher for the RL3 than that for the YL3, their integrated over time intensities are close to each other at $P_0 = 10^{21}$ cm^{-2} s^{-1}. For the RL3 component, the linear dependence at low excitation intensities changes to complete saturation at $P_0 \approx 10^{20}$ cm^{-2} s^{-1} and starts increasing again at $P_0 > 10^{22}$ cm^{-2} s^{-1}. The YL3 component cannot be reliably resolved below $P_0 \approx 10^{20}$ cm^{-2} s^{-1}. This agrees with the SSPL data, according to which the YL3 intensity is at least 20 times lower than the RL3 intensity at 100 K. Between $P_0 = 10^{20}$ and 10^{21} cm^{-2} s^{-1}, the YL3 intensity sharply increases, and at higher excitation intensities it shows a sublinear rise. The interplay of the RL3 and YL3 components with increasing excitation intensity is very similar in different samples. An important observation is that the sharp rise of the YL3 intensity coincides with the beginning of the RL3 saturation.

The sum of the RL3 and YL3 components behaves as expected for a simple acceptor in n-type GaN (Fig. 14). This excitation intensity dependence can be explained using a model previously applied to the YL1 band (related to the C_N acceptor) [7] and the BL1 band (related to the Zn_{Ga} acceptor) [20]. An example is shown in Fig. 14, where the solid line is calculated numerically with the assumption that the laser excitation intensity decreases exponentially as it travels from the sample surface to the bulk (the advanced model). By
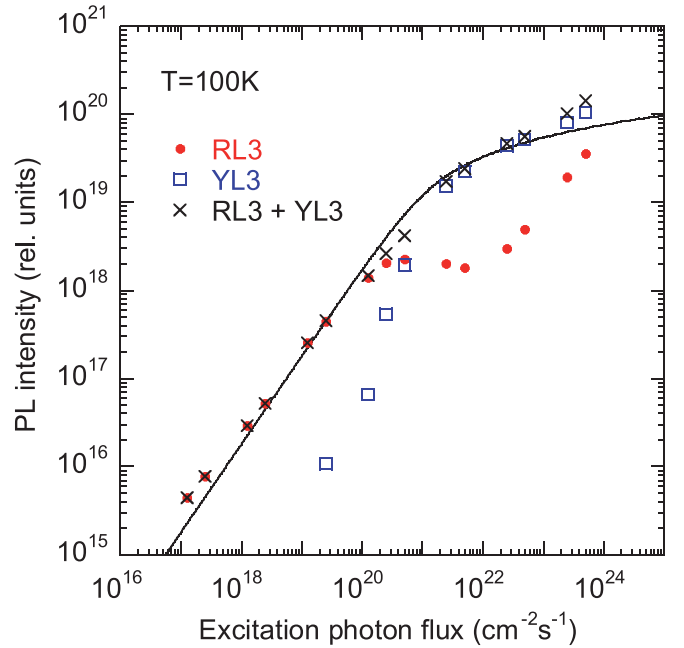

FIG. 14. Time-integrated PL intensity as a function of the excitation intensity for the RL3 and YL3 components and their sum in sample H106 at $T = 100$ K. The solid line is calculated numerically with $N_i = 1.5 \times 10^{16}$ cm^{-3}.

assuming that the excitation intensity of the laser is constant between the surface and the "edge" of the effective PL layer (the simple model), an analytical expression can be used to find N_i from the parameter $P_i^{\mathrm{cr,TRPL}}$, the point at which the PL intensity in TRPL switches from a linear rise to saturation with increasing laser intensity [20]:

$$P_i^{\mathrm{cr,TRPL}} = \frac{N_i}{\eta_{0i}\alpha t_L}, \qquad (13)$$

where t_L is the duration of the laser pulse ($t_L \approx 1$ ns in our experiment). Note that $P_i^{\mathrm{cr,TRPL}}$ is independent of PL lifetime. For sample H106, we obtain $N_{\mathrm{RY3}} = 1.5 \times 10^{16}$ cm^{-3} from the numerical solution in the advanced model and $N_{\mathrm{RY3}} = 3 \times 10^{16}$ cm^{-3} from Eq. (12) using the simple model. These values are close to the value found from SSPL data above ($N_{\mathrm{RL3}} \approx 1 \times 10^{16}$ cm^{-3}).

Due to an unusually short lifetime of the RL3 component, it could be detected in numerous GaN samples grown by the HVPE method, even in samples where this PL band is hidden under very intense RL1 (to be discussed in Sec. IV A) and YL1 bands in the SSPL spectra. Figure 15 shows the PL intensity integrated over time for the RL1, YL1, and RL3 bands in one of such samples (H201). The SSPL and TRPL spectra for this sample can be found in Refs. [9,10]. The very weak RL3 component could be detected only in TRPL. By comparing the TRPL data for sample H201 with that for samples which have intense RL3 emission (such as H106), we have estimated that the concentration of the RY3 center in sample H201 is only about 10^{13} cm^{-3}.
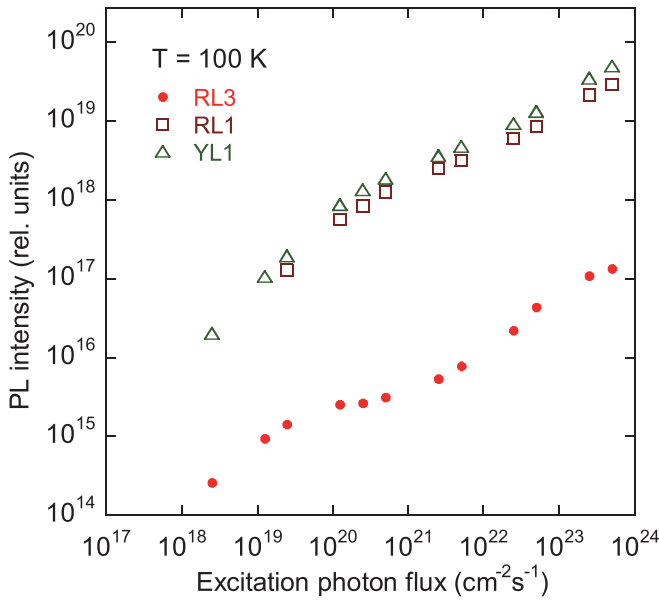
FIG. 15. Time-integrated PL intensity as a function of the excitation photon flux for the RL3, RL1, and YL1 bands in sample H201 at $T = 100$ K.

IV. DISCUSSION

A. Red luminescence bands in undoped GaN

From the analysis of a large number of GaN samples, we conclude that there are three PL bands related to different defects that may appear in the red portion of the PL spectrum of undoped GaN (RL1, RL2, and RY3 bands) [4,9,10,24]. The RL1 band in conductive *n*-type GaN grown by HVPE is caused by transitions from shallow donors (at low temperatures) or from the conduction band (at temperatures above 50–100 K) to an unknown acceptor with a level at about 1.2 eV above the valence band. The electron capture coefficient C_{ni} and the hole capture coefficient C_{pi} for this acceptor are $(4.3 \pm 0.4) \times 10^{-14}$ and $(2.9 \pm 0.7) \times 10^{-7}$ cm^3/s, respectively [7]. At low temperatures (below 50 K), the decay of the RL1 band is nonexponential due to DAP-type transitions involving shallow donors and deep acceptors. At $T > 50$ K, the PL decay is slow and nearly exponential. The corresponding PL lifetime is inversely proportional to the concentration of free electrons [9]. The very long PL lifetime (typically around 1 ms) [4,9,25] is the distinguishing feature of the RL1 band. It is also likely that our RL1 band is the same as the red luminescence band in freestanding, HVPE-grown GaN studied by optically detected magnetic resonance (ODMR), which revealed an acceptor-like isotropic magnetic resonance with $g = 2.019$ [26].

The RL2 band is observed only in semi-insulating GaN, usually grown in very Ga-rich conditions. This band is caused by internal transitions (from an excited state to the ground state of the same defect) in an unknown defect [4]. It is more often observed in semi-insulating GaN grown by molecular beam epitaxy (MBE), and it can be recognized by an exponential and slow decay after a laser pulse. The PL lifetime decreases from 110 to 2 μs with increasing temperature from 15 to 100 K [24]. Due to the characteristic change in PL lifetime with temperature, the RL2 intensity may show a significant

increase with increasing temperature unless the measurements are conducted at very low excitation intensity [27,28]. The decreasing PL intensity with decreasing temperature can be explained by the partial saturation of PL intensity at temperatures below ~50–100 K due to increasing PL lifetime, and the increase is not observed if the measurements are taken at very low excitation intensity [4].

The RY3 band can be found in nearly all *n*-type GaN samples grown by HVPE. Even when the concentration of the related defect is very low, the RY3 band can be detected due to its unusually fast decay after a laser pulse. It can also be recognized by its unusual shape: a shoulder at the high-energy side (the YL3 component) that cannot be resolved as a separate PL band by changing excitation intensity or temperature. In the literature, the RY3 band with its characteristic shape was observed in GaN samples grown by HVPE and containing high concentrations of oxygen and carbon ($\sim 10^{19}$ cm^{-3}) [12,13]. In these works, the red luminescence band was attributed to O and C. However, in some of our undoped GaN samples with an intense RY3 band, the concentrations of these impurities from SIMS analysis are extremely low (e.g., [C] $< 10^{15}$ cm^{-3} and [O] $= 10^{16}$ cm^{-3} for sample RS280). The RL3 component can be recognized by its fast and exponential decay after a laser pulse. It is likely that the red luminescence with a PL lifetime of 12 ns at $T = 2$ K in GaN samples grown by HVPE (Ref. [29]) is the RY3 band.

The RL3 and YL3 components always appear together and form the unusual shape of the RY3 band. The temperature dependences of the RL3 and YL3 components are also unusual, especially the increase of the YL3 component with temperature. It is known that in samples with a PL band which has a very high quantum efficiency, the thermal quenching of this band causes a concurrent rise in the intensities of all other PL bands. This phenomenon is explained in a multi-center model by a competition of recombination channels for nonequilibrium holes in an *n*-type semiconductor [16,30]. However, the rise of the YL3 intensity concurrently with the quenching of the RL3 component in temperature-dependent SSPL (Fig. 5) cannot be explained by this mechanism. Indeed, only the YL3 component increases in the temperature range of 100–200 K, whereas the exciton band intensity decreases monotonously with increasing temperature in this sample (Fig. 5). Moreover, the increase of the YL3 intensity is identical in samples which have very different contributions of the RY3 band to the SSPL spectrum. The interplay of the YL3 and RL3 components with increasing excitation intensity in TRPL is also identical in different samples. Finally, the thermal quenching of the RL3 and YL3 components occurs in the same temperature range and with the same activation energy. All these facts indicate that the RL3 and YL3 components originate from the same defect, the RY3 center. To explain the unusual properties of the RY3 center, we propose the following model.

B. Model of the RY3 center

The experimental results, presented in Sec. III, can be explained with the following model of the RY3 center (Fig. 16). The RY3 center is an acceptor with a very deep ground state: the corresponding $-/0$ charge transition level, A_1, is located at 0.5–1.0 eV below the conduction band. The bound hole in
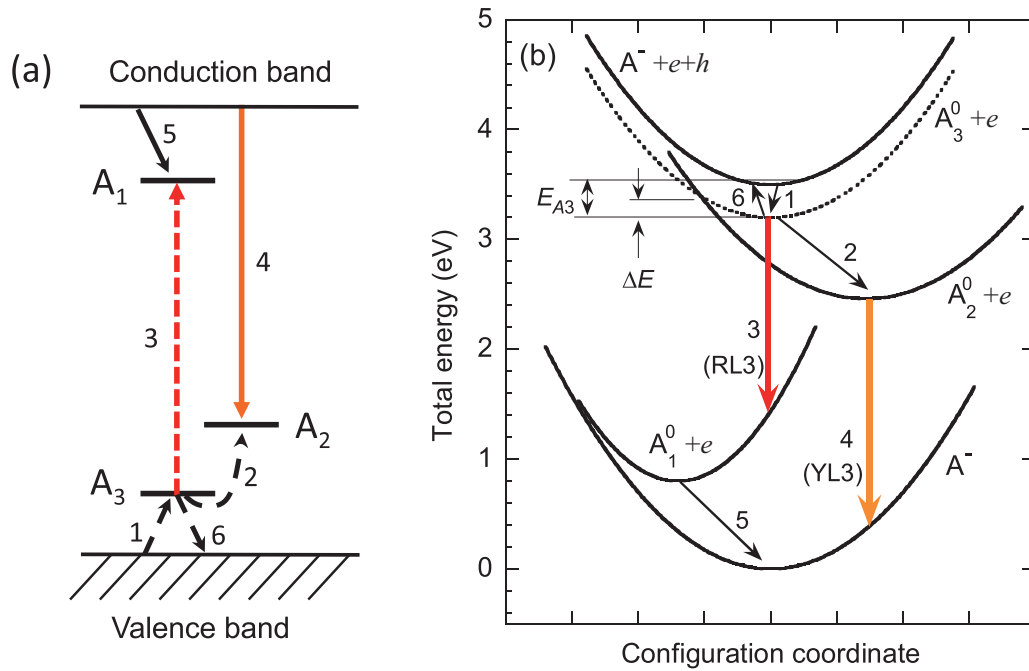
FIG. 16. Schematics of transitions associated with the RY3 band in GaN. (a) Band diagram. (b) Configuration coordinate diagram. A^- is the ground state of the RY3 center in n-type GaN (negatively charged acceptor); A_1^0 is the ground state of the neutral acceptor with a strongly localized hole, A_2^0 is the deep excited state with a localized hole, and A_3^0 is the shallow excited state with a weakly localized hole. The transitions 3 and 4 are responsible for the RL3 and YL3 components of the RY3 band.

this state is strongly localized, possibly in the d-shell of a transition metal impurity. In n-type GaN, this level is filled with electrons in equilibrium, and the defect is negatively charged. After band-to-band excitation, a photogenerated hole in the valence band is first captured at the delocalized, diffuse state, A_3, with the level located at about 0.2 eV above the valence band; this is the nonradiative transition 1 with a characteristic time of $\sim$0.1 ns (see Appendix), depending on the concentration of RY3 centers. The transition from the excited state, A_3, to the ground state, A_1, (the radiative transition 3 with $\tau^{PL} \approx 10$ ns) is internal, allowed, and occurs without changing the charge of the defect. This transition of the bound hole from the shallow excited state to the ground state of the acceptor causes the RL3 component with a maximum at 1.77 eV, for which the ZPL is predicted to reside at 2.3–2.5 eV based on the component shape on its high-energy side. This case is similar to the Cu-related green band with a ZPL at 2.859 eV in ZnO, which is caused by internal transitions of holes from an excited state of the Cu_{Zn} acceptors to the ground state located close to the conduction-band minimum [31]. The slowest and the last step in the recombination cycle involving the RL3 emission is the capture (most likely nonradiative) of a free electron by the acceptor in a neutral state (transition 5 with the characteristic time $\tau_{n1} \approx 20 - 60\,\mu$s).

To explain the link between the RL3 and YL3 components, we propose that the RY3 center has an additional excited state (A_2) with a strongly localized hole and an energy level at 1.13 eV above the valence band. The direct capture of a photogenerated hole by the A_2 state is less likely than capture via the diffuse state A_3 (transition 1 followed by transition 2). Furthermore, the hole in the A_2 state recombines with an electron at a nearby shallow donor (DAP-type transition 4') at

low temperatures or with a free electron (radiative transition 4 with $\tau^{PL} \approx 200\,\mu$s) at $T > 50$ K. The electron-hole recombination via the A_2 state causes the YL3 component with a maximum at 2.07 eV and ZPL at 2.36 eV (DAP recombination at $T < 30$ K) or 2.38 eV (eA recombination at $T > 50$ K). The PL lifetime of the YL3 band is inversely proportional to n at $T > 50$ K, and the YL3 intensity decay is nonexponential at $T = 18$ K. These facts confirm the assignment of the YL3 component to electron transitions from the conduction band to the acceptor level located at 1.13 eV at $T > 50$ K and to DAP recombination involving shallow donors and the same acceptor at $T < 50$ K.

An interesting feature of the model is that the hole at the shallow excited state, A_3, can transfer to the A_2 state (transition 2) with a probability exponentially depending on temperature due to a potential barrier with an effective height of 0.06–0.07 eV between these two states. At $T < 90$ K, a tunneling transition through the barrier occurs with a characteristic time $\tau_{32} \approx 500$ ns. This is much longer than the characteristic time of radiative transition 3 ($\tau_{31} \approx 10$ ns). The ratio τ_{32}/τ_{31} determines the ratio between the RL3 and YL3 intensities in the SSPL at low temperatures (Fig. 5), see the Appendix. At $T > 90$ K, thermally activated transitions over the barrier explain the exponential rise in the YL3 intensity and simultaneous decrease of the RL3 intensity, both with an activation energy of about 0.06 eV. At $T = 200$ K, the probabilities of transitions 2 and 3 become almost equal ($\tau_{32} \approx 20$ ns and $\tau_{13} \approx 10$ ns), and the relative contributions of the RL3 and YL3 components to the RY3 band are nearly equal between 200 and 300 K. Note that the RL3 lifetime, as measured in TRPL experiment, is affected by τ_{32}, because transitions 2 and 3 occur in parallel. The states A_2 and A_1

are probably separated by a high barrier, or the transitions from A_2 to A_1 are forbidden and very slow, so that they can be ignored. Otherwise, transitions between these states would shunt transitions 4 and 4′ that are responsible for the slow YL3 component.

At $T = 18 - 80$ K, in the limit of low excitation intensities in SSPL, both the RL3 and YL3 components (the latter is reliably distinguished due to its ZPL at 2.36–2.38 eV) increase linearly with excitation intensity (Fig. 11). Thus these components cannot be related to two different charge states of the defect, because capture of the second hole by the same defect can be ignored in the limit of low excitation intensity [7]. At high excitation intensity ($P_0 > 10^{16}$ cm^{-2} s^{-1}), saturation of the YL3 and RL3 emissions begins in SSPL. The saturation of the RL3 channel begins first due to its much higher quantum efficiency, and the limiting step causing this saturation is the relatively slow capture of free electrons by the A_1 state ($\tau_{n1} \approx 30 \, \mu$s). We can speculate that the electron transition is nonradiative but slow, because it is forbidden, or it has a barrier. Alternatively, it could be radiative, with emission expected in the far infrared region. The saturation of the YL3 intensity in the SSPL is associated with the long lifetime of the bound hole in the A_2 state ($\tau_{0,\text{YL3}} \approx 200 \, \mu$s). It is important to note that the saturation of the RL3 and YL3 components in SSPL with increasing excitation intensity at $T < 200$ K is limited by slow transitions 5 and 4, respectively (Fig. 16), while the A_3 state cannot be saturated with holes in our SSPL experiments, because holes escape from this state very quickly, with the characteristic time $\tau_{0,\text{RL3}} = \tau^* \approx 10$ ns.

At $T > 200$ K, the thermal emission of holes from the A_3 state to the valence band becomes noticeable. As a result, intensities of the YL3 and RL3 components decrease with temperature simultaneously and with an activation energy of about 0.2 eV. The measured PL lifetime of the RL3 component also decreases with the same activation energy at $T > 200$ K. This is because, after a hole is captured by the A_3 state, it may be emitted back to the valence band in time, τ_{A3}^{th}, shorter than $\tau_{0,\text{RL3}} = \tau^*$, after which it recombines with electrons via other recombination channels. At $T > 400$ K, the quenching of the RY3 band occurs with higher activation energy (0.5 eV or higher). This process can be explained by the thermal emission of electrons from the A_1 state to the conduction band.

The behavior of TRPL with increasing excitation intensity is unusual, especially the very abrupt saturation of the RL3 component in Fig. 14, and it appears to contradict the SSPL behavior. Indeed, in TRPL, the superlinear increase of the YL3 intensity is observed in the region where the RL3 component saturates (Figs. 13 and 14), while both components

saturate similarly and at about the same excitation intensity in SSPL (Fig. 11). The difference between the PL saturation in TRPL and SSPL experiments is that the saturation of the RL3 intensity in TRPL experiment is caused by the saturation of the A_3 level with holes during a short but intense laser pulse, whereas the saturation of the YL3 and RL3 intensities in SSPL experiment is caused by the saturation with holes of the A_2 and A_1 levels, respectively (see Appendix). We also note that the superlinear increase of the YL3 intensity in TRPL experiment *cannot* be explained with the assumption that the A_2 state is the 0/+ transition level of the RY3 defect and that the YL3 emission occurs after two holes are captured by the defect. If this was the case, the superlinear (nearly quadratic) increase of the YL3 band would be observed in SSPL experiments as well. However, the YL3 component, whose ZPL is well-resolved at $T = 18$ K, decreases *linearly* with decreasing excitation intensity in SSPL, for a very wide range of excitation intensities (Fig. 11). Further studies are under way to clarify the details of unusual TRPL behavior.

C. Identification of the RY3 center and other defects

The RY3 center is a point defect, more or less uniformly distributed in the bulk region of the sample. To confirm this assumption, we conducted two types of experiments. In the first one, a 10-μm-thick GaN sample (H101) with a strong RY3 band was illuminated with the HeCd laser from the backside, through a double-polished sapphire substrate. The RY3 band was clearly observed in SSPL and TRPL spectra, along with the Zn-related BL1 band (not detected from the front surface). In another experiment, the top 100-nm layer of GaN (H106) was removed by inductively coupled plasma etching. However, the PL spectrum and intensity of the RY3 band did not change.

From the analysis of the results presented in this work, it can be concluded with confidence that the RY3 center is an acceptor. Among the arguments in favor of this conclusion are the DAP-type behavior of the YL3 component, the very high quantum efficiency and fast capture of holes by the RY3 center in n-type GaN where photogenerated holes are minority carriers. In order to find impurities that may be responsible for the RY3 band, SIMS measurements on selected samples were conducted by Evans Analytical Group. The results are shown in Table I. These data can be compared with the concentrations of free electrons and defects determined from PL, the Hall effect, and PAS, which are shown in Table II.

The total concentration of Si and O, which are shallow donors in GaN ($\sim 10^{16}$ cm^{-3} in sample RS280 and $\sim 10^{17}$ cm^{-3} in other samples), agrees with the concentrations

TABLE I. Concentrations of impurities (in 10^{15} cm^{-3} units) in GaN from SIMS analysis.

Sample	[C]	[O]	[Si]	[Cl]	[H]	[Fe]	[Ni]	[Cr]	[V]	[Mn]	[Mg]	[Zn]
H102	<2	20	30	<1	<500							
H106	<2	70	20	2	<500	2.5	<5	<0.08	<0.07	<0.3		
H202	<2	<10	80	40	<500	<0.7	<5	<0.08	<0.07	<0.3		
H2057	<5	23	45	30	<200							
RS280	<1	10	<2	8	<200						<2	<15
Detection limit	1–5	3–10	2–10	1	200–500	0.7	5	0.08	0.07	0.3	2	15

TABLE II. Concentrations of free electrons and defects (in 10^{15} cm^{-3} units) in GaN from PL, Hall effect, and PAS analyses.

Sample	Photoluminescence					Hall effect	PAS
	N_{RY3} (RY3)	[Mg$_{Ga}$] (UVL)	[Zn$_{Ga}$] (BL1)	[C$_N$] (YL1)	n (100K)	n (250K)	[V$_{Ga}$]
H102	10	0.3	0.03	<0.1	15	46	40
H106	10	0.3	0.03	<0.1	13	35	15
H202	0.01	0.03	0.001	0.5	34	61	140
H2057	0.01	0.01	0.0001	2	31	54	1000
RS280	0.2	0.1	1	<0.1	3		10

of free electrons determined from PL and Hall effect measurements, and this comparison predicts that the concentration of all acceptors does not exceed $\sim 5 \times 10^{16}$ cm^{-3} in the studied samples and even lower in sample RS280. The Mg$_{Ga}$, Zn$_{Ga}$, and C$_N$ acceptors are responsible for the UVL, BL1, and YL1 bands, respectively, and are unlikely to cause the RY3 band. The concentrations of these impurities are below the detection limit of SIMS, yet they can be reliably estimated from PL measurements. A commonly considered acceptor in GaN is the gallium vacancy (V$_{Ga}$), isolated or forming complexes with O, H, Si and/or V$_N$ [32–34]. However, it is unlikely that the V$_{Ga}$ defect is responsible for the RY3 center. Indeed, the concentration of V$_{Ga}$-related defects in sample H2057 is about two orders of magnitude higher than in sample H106, while the RY3 intensity is three orders of magnitude stronger in sample H106 (Table II).

If we consider acceptors which are specific to HVPE growth, transition metals or their complexes with hydrogen seem to be the main candidates for the RY3 center. One reason is that the RY3 center is a very deep acceptor with two excited states, and this resembles properties of transition metals in GaN and other semiconductors [35,36]. Another reason is that transition metals are sometimes present in undoped GaN grown by HVPE, possibly due to specific growth conditions. In particular, Baur *et al.* [37] detected vanadium (V^{3+}) in most GaN samples grown by HVPE but never in MOCVD samples. Low levels of Fe (3×10^{15} cm^{-3}) [38] and Cr (2×10^{14} cm^{-3}) [39] were found in high-quality, bulk, undoped HVPE GaN. Hydrogen is also a common contaminant in this growth method.

It is possible that the reaction of HCl active gas (having traces of water vapor) with hot stainless steel parts, such as a flange in the HVPE reactor, causes contamination of GaN with Fe, Ni, and Cr. To test this hypothesis, we conducted more detailed SIMS analysis of sample H106 (high concentration of the RY3 centers) and H202 (very low concentration). The concentration of Fe is indeed elevated in sample H106; the contamination with Cr is very low; and the detection limit of Ni is too high to exclude this impurity from the candidates for the RY3 defect (Table I). Note that the concentration of the RY3 center in sample H106 (1×10^{16} cm^{-3}) has been found from analysis of PL (Sec. IIID), where the error may reach half an order of magnitude due to uncertainty in the absolute internal quantum efficiency [7,15]. We have estimated that $\eta_{RY3} = 0.3$ in sample H106 at $T = 80$ K by comparing the PL intensity with that from calibrated GaN samples. It cannot be much larger than 0.3 (perhaps, $\eta_{RY3} < 0.6$), because otherwise we would see a stepwise rise of the exciton emission

intensity (by a factor of 1.5 or larger) at about 200 K, when the RY3 band begins to quench (Fig. 5). On the other hand, it cannot be much lower than 0.3, because the integrated intensity of the RY3 band is close to that of the YL1 band in GaN:C where $\eta_{YL1} = 0.8 \pm 0.1$ [7]. Accounting for this uncertainty in $\eta_{RY3} = 0.3$, we estimate that the lower bound of the concentration of the RY3 center in samples H102 and H106 is 3×10^{15} cm^{-3}. In conclusion, Fe and Ni appear to be the most likely sources for the RY3 defect. Note that the defect may be a complex. Puzyrev *et al.* [40] predict that formation energy of a Fe$_{Ga}$V$_N$ complex is significantly lower than that of the isolated Fe$_{Ga}$ defect. The complexes may also involve O$_N$, or H$_i$, which complicates the identification.

In the literature, the Fe$_{Ga}$ acceptors are considered to be centers of *nonradiative* recombination in GaN samples heavily doped with Fe, which are semi-insulating [41,42]. Nevertheless, it is instructive to recall a situation with the UVL band in Mg-doped GaN, which is caused by electron transitions from the conduction band to the Mg$_{Ga}$ level located at 0.2 eV above the valence band. The UVL band intensity increases linearly with increasing concentration of Mg up to $\sim 10^{16}$ cm^{-3} in conductive n-type GaN [15]. However, in p-type or semi-insulating GaN with a Mg concentration of about 10^{19} cm^{-3}, the UVL intensity is orders of magnitude lower than in n-type and sometimes is not observed at all [19]. Although the transitions via the Mg$_{Ga}$ are radiative (the UVL band), their efficiency dramatically drops with increasing concentration of Mg. The main reason for this drop is the abrupt shift of the Fermi level and related changes in recombination flows [16,19].

V. SUMMARY

We have shown that the broad RY3 band with a maximum at 1.8 eV in GaN samples grown by HVPE consists of slow YL3 and fast RL3 components with identical relative contributions in different samples, indicating that both components belong to one defect, the RY3 center. In SSPL, the YL3 intensity increases and the RL3 intensity decreases with increasing temperature from 100 to 200 K. The characteristic interplay of the RL3 and YL3 components is also observed in TRPL, where a sharp rise of the YL3 intensity occurs when the RL3 component saturates with increasing excitation intensity.

In SSPL, at temperatures below 90 K, photogenerated holes are captured with high efficiency by the excited, effective-mass state of the RY3 center, the A$_3$ level located at 0.2 eV above the valence-band maximum. The hole-capture coefficient for the A$_3$ state is $\sim 10^{-7} - 10^{-5}$ cm^3/s. A hole

at the A_3 level transitions to the ground state A_1 located at 2.7 ± 0.2 eV above the valence band, with a characteristic time of 8–10 ns. This transition produces the RL3 component with a maximum at 1.8 eV. The electron-hole recombination cycle of this type ends with the capture of a free electron at the A_1 level. This transition is relatively slow (the lifetime is 20–60 μs). The hole at the A_3 level may also transition to a deeper excited state, A_2, located at 1.13 eV above the valence band. The hole stays at the A_2 level for about 200–400 μs and then recombines with an electron at the nearest shallow donor (DAP-type transition) or with a free electron (eA transition). These transitions produce the YL3 component with a maximum at 2.1 eV and ZPL at 2.36 eV. A barrier with the effective height of 0.06 eV exists between the A_3 and A_2 states. At low temperatures ($T < 90$ K), only tunneling is possible, and the YL3 component is weak ($\sim 5\%$ of the RY3 component). With increasing temperature from 90 to 180 K, the rate of transition from the A_3 level to the A_2 level increases exponentially, and the relative contribution of the YL3 component to the overall RY3 band increases by a factor of ~ 7, while the contribution of the RL3 component decreases. We preliminarily suggest that Fe_{Ga} or Ni_{Ga}, or their complexes with O, H, and vacancies, could be the origin of the RY3 band. While the RY3 band is very strong in some undoped GaN samples grown by HVPE (where the concentration of the RY3 center is close to 10^{16} cm^{-3}), this defect can be detected in nearly all *n*-type GaN samples grown by this method due to the unusually short lifetime of the RL3 emission. The defect resembles a giant trap with very efficient trapping of nonequilibrium holes. Thus, even low concentrations of this defect, much lower than the SIMS detection limit, may cause a detrimental effect on the performance of GaN-based devices.

APPENDIX: RATE-EQUATION MODEL

The dependences of PL intensity on temperature and excitation intensity can be explained by using phenomenological models that proved to be very fruitful for explaining PL behavior in GaN [16,19,20]. Transitions for the proposed model are shown in Fig. 1. For simplicity, transitions via shallow donors D (arrow 4$'$) will be ignored, which is justified for temperatures above 50 K, when transitions from the conduction band dominate over DAP transitions. A nonradiative defect S with concentration N_S must be included to explain the less than 100% quantum efficiency of PL and the PL quenching with increasing temperature. For definiteness, the S center is a deep acceptor, yet the results below will not change if it is a deep donor. N_S^- and N_S^0 are the concentrations of the S center in two charge states, N_{A1}^0, N_{A2}^0, and N_{A3}^0 are the concentrations of the neutral RY3 acceptor with a bound hole in the A_1, A_2, and A_3 states, respectively, and N_A^- is the concentration of negatively charged RY3 acceptors. The total concentration of the RY3 centers is $N_A = N_{A1}^0 + N_{A2}^0 + N_{A3}^0 + N_A^-$. First, low excitation intensities (before saturation of PL) will be considered, when $N_A^- \approx N_A$ and $N_S^- \approx N_S$.

The rate equation involving transitions to and from the conduction band in steady state is

$$G = \frac{N_{A1}^0}{\tau_{n1}} + \frac{N_{A2}^0}{\tau_{n2}} + \frac{N_S^0}{\tau_{nS}}, \tag{A1}$$

where G is the electron-hole generation rate, $\tau_{n1} = (C_{n1}n)^{-1}$, $\tau_{n2} \equiv \tau_{0,\text{YL3}} = (C_{n2}n)^{-1}$, and $\tau_{nS} = (C_{nS}n)^{-1}$ are the characteristic times of transitions 5, 4, and 7, respectively (Fig. 1), C_{n1}, C_{n2}, and C_{nS} are the electron-capture coefficients for these transitions, and n is the concentration of free electrons. The rate equation involving transitions to and from the valence band is

$$G = \frac{p}{\tau_{p3}} + \frac{p}{\tau_{pS}} - \frac{N_{A3}^0}{\tau_{A3}^{\text{th}}}, \tag{A2}$$

where $\tau_{p3} = (C_{p3}N_A)^{-1}$ and $\tau_{pS} = (C_{pS}N_S)^{-1}$ are the characteristic times of hole capture by the excited state A_3 of the RY3 center and the S center, respectively (transitions 1 and 8), C_{p3} and C_{pS} are the hole-capture coefficients for these defects, p is the concentration of free holes. τ_{A3}^{th} is the characteristic time of the thermal emission of holes from the A_3 state to the valence band (transition 6) [19]:

$$\tau_{A3}^{\text{th}} = \frac{g \exp\left(\frac{E_{A3}}{kT}\right)}{C_{p3}N_v}. \tag{A3}$$

Here, E_{A3} is the energy of the A_3 state relative to the valence-band maximum, N_v is the effective density of states in the valence band, and g is degeneracy of the A_3 state.

For transitions via the A_1 level:

$$\frac{N_{A1}^0}{\tau_{n1}} = \frac{N_{A3}^0}{\tau_{31}}, \tag{A4}$$

where τ_{31} is the characteristic time of transition 3. For transitions via the A_2 level (ignoring DAP-type transitions):

$$\frac{N_{A2}^0}{\tau_{n2}} = \frac{N_{A3}^0}{\tau_{32}}, \tag{A5}$$

where τ_{32} is the characteristic time of transition 2. For transitions via the A_3 level:

$$\frac{p}{\tau_{p3}} = \frac{N_{A3}^0}{\tau_{31}} + \frac{N_{A3}^0}{\tau_{32}} + \frac{N_{A3}^0}{\tau_{A3}^{\text{th}}}. \tag{A6}$$

The nonradiative transition 2 occurs via a barrier with the height ΔE [Fig. 15(b)]. Then

$$(\tau_{32})^{-1} = \nu_0 + \nu_1 \exp\left(-\frac{\Delta E}{kT}\right), \tag{A7}$$

where ν_1 is the probability of transition from A_3 to A_2 in the absence of the barrier (it can also be considered as the effective frequency of vibrations in the zero level of the A_3 state), and the coefficient ν_0 accounts for tunneling through the barrier at very low temperatures.

In *n*-type semiconductors, holes are minority carriers, and the efficiency of electron-hole recombination is governed by the rates of hole capture by different defects. At low temperatures, when the terms containing τ_{A3}^{th} can be ignored, the absolute quantum efficiency of PL from the RY3 center,

$\eta_0 \equiv \eta_{0,\mathrm{RY3}}$, can be found from Eq. (A2) as

$$\eta_0 = \frac{\tau_{pS}}{\tau_{p3} + \tau_{pS}}. \tag{A8}$$

Note that η_0 can be found experimentally by using methods described in Refs. [15–17].

For any temperature, the variable p can be expressed from Eq. (A2) and substituted into Eq. (A6), accounting for Eq. (A8), which results in

$$N_{A3}^0 = \frac{\eta_0 G}{\frac{1}{\tau_{31}} + \frac{1}{\tau_{32}} + \frac{(1-\eta_0)}{\tau_{A3}^{\mathrm{th}}}}. \tag{A9}$$

The intensity of the RL3 component (transition 3) is

$$I^{\mathrm{RL3}} = \frac{N_{A3}^0}{\tau_{31}} = \frac{\eta_0 G}{1 + \frac{\tau_{31}}{\tau_{32}} + \frac{\tau_{31}(1-\eta_0)}{\tau_{A3}^{\mathrm{th}}}}, \tag{A10}$$

and that of the YL3 component (transition 4), accounting for Eq. (A5), is

$$I^{\mathrm{YL3}} = \frac{N_{A2}^0}{\tau_{n2}} = \frac{N_{A3}^0}{\tau_{32}} = \frac{\eta_0 G}{1 + \frac{\tau_{32}}{\tau_{31}} + \frac{\tau_{32}(1-\eta_0)}{\tau_{A3}^{\mathrm{th}}}}. \tag{A11}$$

At temperatures lower than the beginning of the RY3 band quenching ($T < 200$ K):

$$I^{\mathrm{RL3}}(0) + I^{\mathrm{YL3}}(0) = \frac{N_{A3}^0}{\tau_{0,\mathrm{RL3}}} = \eta_0 G, \tag{A12}$$

where

$$\frac{1}{\tau_{0,\mathrm{RL3}}} = \frac{1}{\tau^*} = \frac{1}{\tau_{31}} + \frac{1}{\tau_{32}}. \tag{A13}$$

Note that, while τ_{31} is the characteristic time of transition responsible for the RL3 component, the decay of the RL3 emission after a laser pulse is shunted by competing transitions from A_3 to A_2, which occurs with the characteristic time τ_{32}. As a result, PL lifetime of the RL3 emission *measured* in TRPL experiments at $T < 200$ K is $\tau_{0,\mathrm{RL3}} = \tau^*$.

The ratio between the RL3 and YL3 intensities can be found from Eqs. (A10) and (A11) as

$$\frac{I^{\mathrm{YL3}}}{I^{\mathrm{RL3}}} = \frac{\tau_{31}}{\tau_{32}} = \tau_{31}\left[\nu_0 + \nu_1 \exp\left(-\frac{\Delta E}{kT}\right)\right], \tag{A14}$$

which becomes $I^{\mathrm{YL3}}(0)/I^{\mathrm{RL3}}(0) = \tau_{31}\nu_0$ in the limit of low temperatures.

Equations (A10) and (A11) can be rewritten as

$$\eta_{\mathrm{RL3}}(T) = \frac{I^{\mathrm{RL3}}(T)}{G} = \frac{\eta_{0,\mathrm{RL3}}}{1 + C_1 \exp\left(-\frac{E_1}{kT}\right) + C_2 \exp\left(-\frac{E_2}{kT}\right)} \tag{A15}$$

and

$$\eta_{\mathrm{YL3}}(T) = \frac{I^{\mathrm{YL3}}(T)}{G}$$
$$= \eta_{0,\mathrm{YL3}} \frac{1 + C_3 \exp\left(-\frac{E_1}{kT}\right)}{1 + C_1 \exp\left(-\frac{E_1}{kT}\right) + C_2 \exp\left(-\frac{E_2}{kT}\right)}, \tag{A16}$$
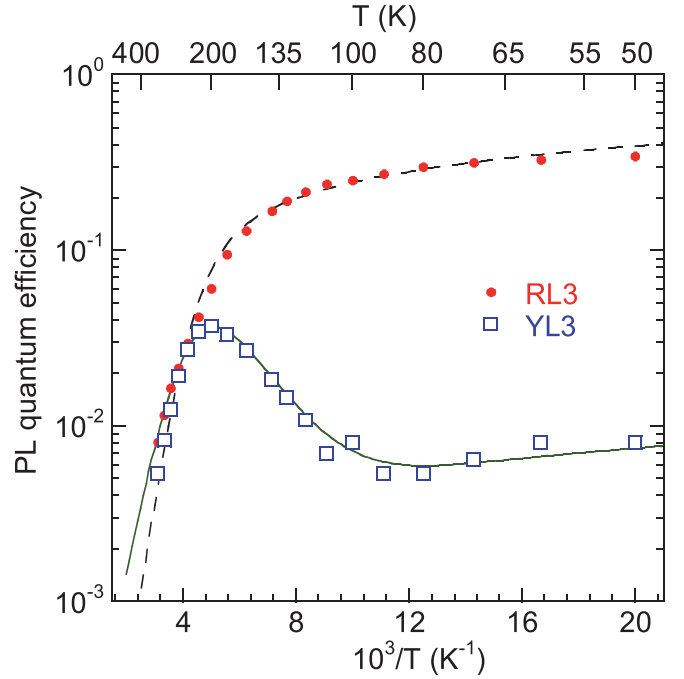

FIG. 17. Temperature dependence of PL quantum efficiency for the RL3 and YL3 components of the RY3 band (sample H106, $P_{\mathrm{exc}} = 10^{-4}$ W/cm^2). The dashed and solid lines are calculated using Eqs. (A10) and (A11), respectively, with the following parameters: $\Delta E = 0.07$ eV, $E_{A3} = 0.2$ eV, $\tau_{31} = 10$ ns, $\tau_{p3}/\tau_{pS} = 1.6(T/T^*)$, $C_{p3} = 6 \times 10^6 (T^*/T)$ cm^3/s, $T^* = 50$ K, $\nu_0 = 2 \times 10^6$ s^{-1}, $\nu_1 = 3 \times 10^9$ s^{-1}, $N_v = 3.2 \times 10^{15} T^{3/2}$ cm^{-3}, and $g = 2$.

where $E_1 = \Delta E$, $E_2 = E_{A3}$, $C_1 = \tau_{31}\nu_1(1 + \tau_{31}\nu_0)^{-1}$, $C_2 = C_1(1-\eta_0)C_{p3}N_v(g\nu_1)^{-1}$, $C_3 = \nu_1/\nu_0$, $\eta_{0,\mathrm{RL3}} = \eta_0(1 + \tau_{31}\nu_0)^{-1}$, and $\eta_{0,\mathrm{YL3}} = \eta_0\tau_{31}\nu_0(1 + \tau_{31}\nu_0)^{-1}$. Equations (A15) and (A16) are identical to Eq. (1) used above to fit the temperature dependences in Fig. 5. The total quantum efficiency of the RY3 band is

$$\eta_{\mathrm{RY3}}(T) = \eta_{\mathrm{RL3}}(T) + \eta_{\mathrm{YL3}}(T)$$
$$= \eta_0 \frac{1 + C_1 \exp\left(-\frac{E_1}{kT}\right)}{1 + C_1 \exp\left(-\frac{E_1}{kT}\right) + C_2 \exp\left(-\frac{E_2}{kT}\right)}. \tag{A17}$$

Figure 17 shows fits of the temperature dependences for the YL3 and RL3 components with Eqs. (A10) and (A11), which account for temperature dependences of coefficients previously considered to be constant. In this fit, we assumed that the hole capture coefficient for the RY3 center, C_{p3}, decreases linearly with temperature (see the caption to Fig. 17). The decrease can be recognized from several experimental facts (Sec. III D), yet the exact dependence is uncertain, so a linear dependence is chosen for simplicity. Then, τ_{p3} increases linearly with T, and $\tau_{p3} = (C_{p3}N_A)^{-1} = 6 \times 10^{-10}$ s at $T = 50$ K if $N_A = 10^{16}$ cm^{-3}. The parameter η_0 decreases with T [see Eq. (A8)], and it is equal to 0.38 at $T = 50$ K and 0.24 at $T = 100$ K, which agrees with the decrease of η_{RL3} and η_{YL3} with increasing temperature from 50 to 100 K (Fig. 17). The calculated parameter $\tau_{0,\mathrm{RL3}}$ is weakly dependent on T: it decreases from 9.8 to 6.8 ns with increasing temperature from 50 to 200 K, in agreement with the RL3 lifetime dependence (Fig. 10). The parameter τ_{23} decreases from 350 to 19 ns with

increasing temperature from 100 to 200 K, and this decrease is responsible for the rise of the YL3 intensity with activation energy $\Delta E \approx 0.07$ eV in this temperature region. Finally, τ_{A3}^{th} decreases from 38 to 0.6 ns with increasing temperature from 200 to 300 K, and this decrease is responsible for the quenching of the RY3 band and the decrease in PL lifetime of the RL3 component with activation energy $E_{A3} \approx 0.2$ eV in this temperature region.

For transient processes observed in TRPL, Eq. (A6) for transitions via the A_3 level should be rewritten in its general form:

$$\frac{\partial N_{A3}^0}{\partial t} = \frac{p}{\tau_{p3}} - \frac{N_{A3}^0}{\tau_{31}} - \frac{N_{A3}^0}{\tau_{32}} - \frac{N_{A3}^0}{\tau_{A3}^{th}}. \qquad (A18)$$

After a laser pulse, photogenerated holes are captured by the A_3 level very fast (with $\tau_{p3} = 6 \times 10^{-10}$ s, as calculated above). Then the first term on the right side can be ignored if we want to analyze much slower processes described by τ_{31}, τ_{32}, and τ_{A3}^{th}. Recapture of holes emitted from the A_3 level to the valence band by the same level will modify the last term [19], so that Eq. (A18) for times much longer than τ_{p3} becomes

$$\frac{\partial N_{A3}^0}{\partial t} \approx -\frac{N_{A3}^0}{\tau_{31}} - \frac{N_{A3}^0}{\tau_{32}} - \frac{(1-\eta_0)N_{A3}^0}{\tau_{A3}^{th}}. \qquad (A19)$$

The solution of Eq. (A19) is an exponential decay with the characteristic time

$$\tau_{RL3} = \frac{\tau_{0,RL3}}{1 + \frac{(1-\eta_0)\tau_{0,RL3}}{\tau_{A3}^{th}}}, \qquad (A20)$$

compare with Eq. (9). The decay of N_{A3}^0 with time determines the decay of the RL3 component. Thus τ_{RL3} defined by Eq. (A20), and not τ_{31}, is the actual PL lifetime of the RL3 component observed in TRPL experiments.

For transitions via the A_2 level,

$$\frac{\partial N_{A2}^0}{\partial t} = \frac{N_{A3}^0}{\tau_{32}} - \frac{N_{A2}^0}{\tau_{n2}} - \frac{N_{A2}^0}{\tau_{A2}^{th}}. \qquad (A21)$$

Here, we ignore direct capture of photogenerated holes by the A_2 level, but account for the thermal emission of holes from this level to the valence band (with $E_i = 1.13$ eV) or to any excited state not included in the model shown in Fig. 1. After a laser pulse, photogenerated holes are captured by the A_3 level very fast (with $\tau_{32} < 10^{-6}$ s), so that the first term on the right side of Eq. (A21) can be ignored. Similar to the previous case,

we obtain the characteristic time of the N_{A2}^0 decay

$$\tau_{YL3} = \frac{\tau_{n2}}{1 + \frac{(1-\eta_0)\tau_{n2}}{\tau_{A2}^{th}}}, \qquad (A22)$$

which is the actual PL lifetime of the YL3 component observed in TRPL experiments, with $\tau_{n2} \equiv \tau_{0,YL3}$.

By using the above model and parameters, we can also analyze the dependence of PL intensity on the excitation photon flux, $P_0[\text{cm}^{-2}\,\text{s}^{-1}]$, at a fixed temperature ($T = 180$ K) and compare with experiment (sample H106 with $N_A \approx 10^{16}\,\text{cm}^{-3}$). At this temperature, thermal quenching of the RY3 band can be ignored ($\tau_{A3}^{th} \to \infty$), $\tau_{32} \approx 150$ ns, and $\eta_0 \approx 0.15$ for sample H106. In the simple model [7,16], $P_0 = G/\alpha$. With increasing excitation intensity, the parameters N_{A1}^0, N_{A2}^0, N_{A3}^0, N_S^0, and p increase linearly with P_0 until some sort of saturation occurs. The critical excitation photon fluxes in SSPL, P_i^{cr}, i.e., the values of P_0 when the A_1, A_2, and A_3 states become saturated with photogenerated holes, can be roughly estimated by making N_{A1}^0, N_{A2}^0, and N_{A3}^0 equal to N_A. From Eqs. (A4) and (A10) with $\tau_{A3}^{th} \to \infty$ and $N_{A1}^0 = N_A$, we find that the A_1 level can be saturated with holes at

$$P_{A1}^{cr} = \frac{N_A}{\eta_0 \alpha \tau_{n1}}\left(1 + \frac{\tau_{31}}{\tau_{32}}\right) \approx 2 \times 10^{16}\,\text{cm}^{-2}\,\text{s}^{-1} \qquad (A23)$$

where $\tau_{n1} = 30\,\mu$s is the limiting time in the RL3 recombination cycle. Then, the saturation of the RL3 emission in SSPL is expected to begin at $P_0 \approx P_{A1}^{cr} \approx 10^{16}\,\text{cm}^{-2}\,\text{s}^{-1}$ for selected parameters, in agreement with the data in Fig. 11.

From Eq. (A11) with $\tau_{A3}^{th} \to \infty$, $\tau_2 \equiv \tau_{0,YL3} = 200\,\mu$s, and $N_{A2}^0 = N_A$, we find that the A_2 level can be saturated with holes at

$$P_{A2}^{cr} = \frac{N_A}{\eta_0 \alpha \tau_{n2}}\left(1 + \frac{\tau_{32}}{\tau_{31}}\right) \approx 4 \times 10^{16}\,\text{cm}^{-2}\,\text{s}^{-1}, \qquad (A24)$$

and this will cause the saturation of the YL3 component in SSPL (compare with Fig. 11).

Finally, the A_3 level can be saturated with holes in SSPL at

$$P_{A3}^{cr} = \frac{N_A}{\eta_0 \alpha \tau_{0,RL3}} \approx 7 \times 10^{19}\,\text{cm}^{-2}\,\text{s}^{-1}, \qquad (A25)$$

which follows from Eq. (A10) with $\tau_{A3}^{th} \to \infty$ and $N_{A3}^0 = N_A$. For the parameters selected above, the saturation of the A_3 level with holes cannot be achieved in our SSPL experiments ($P_0 < 10^{18}\,\text{cm}^{-2}\,\text{s}^{-1}$). On the other hand, in TRPL, the A_3 level is saturated with holes at

$$P_{A3}^{cr,TRPL} = \frac{N_A}{\eta_0 \alpha t_L} \approx 6 \times 10^{20}\,\text{cm}^{-2}\,\text{s}^{-1}, \qquad (A26)$$

where t_L is the laser pulse length (1 ns). Unlike SSPL, such excitation intensity is readily achieved in TRPL, and the saturation of the RL3 component indeed begins at $P_0 \approx 10^{21}\,\text{cm}^{-2}\,\text{s}^{-1}$ (Fig. 14).

[1] M. W. Doherty, N. B. Manson, P. Delaney, F. Jelezko, J. Wrachtrup, and L. C. L. Hollenberg, Phys. Rep. **528**, 1 (2013).

[2] P. M. Mooney, J. Appl. Phys. **67**, R1 (1990).

[3] D. J. Chadi and K. J. Chang, Phys. Rev. Lett. **60**, 2187 (1988).

[4] M. A. Reshchikov and H. Morkoç, J. Appl. Phys. **97**, 061301 (2005).

[5] J. L. Lyons, A. Janotti, and C. G. Van de Walle, Appl. Phys. Lett. **97**, 152108 (2010).

[6] M. Iwinska, R. Piotrzkowski, W. Litwin-Staszewska, T. Sochacki, M. Amilusik, M. Fijalkowski, B. Lucznik, and M. Bockowski, Appl. Phys. Express **10**, 011003 (2017).

[7] M. A. Reshchikov, M. Vorobiov, D. O. Demchenko, Ü. Özgür, H. Morkoç, A. Lesnik, M. P. Hoffmann, F. Hörich, A. Dadgar, and A. Strittmatter, Phys. Rev. B **98**, 125207 (2018).

[8] T. Narita, K. Tomita, Y. Tokuda, T. Kogiso, M. Horita, and T. Kachi, J. Appl. Phys. **124**, 215701 (2018).

[9] M. A. Reshchikov, J. D. McNamara, M. Toporkov, V. Avrutin, H. Morkoç, A. Usikov, H. Helava, and Yu. Makarov, Sci. Rep. **6**, 37511 (2016).

[10] M. A. Reshchikov, J. D. McNamara, H. Helava, A. Usikov, and Yu. Makarov, Sci. Rep. **8**, 8091 (2018).

[11] M. A. Reshchikov, A. Usikov, H. Helava, and Yu. Makarov, Appl. Phys. Lett. **104**, 032103 (2014).

[12] L. Wang, U. Zeimer, E. Richter, M. Herms, and M. Weyers, Phys. Stat. Sol. a **203**, 1663 (2006).

[13] L. Wang, E. Richter, and M. Weyers, Phys. Stat. Sol. a **204**, 846 (2007).

[14] F. Tuomisto and I. Makkonen, Rev. Modern Phys. **85**, 1583 (2013).

[15] M. A. Reshchikov, A. Usikov, H. Helava, Yu. Makarov, V. Prozheeva, I. Makkonen, F. Tuomisto, J. H. Leach, and K. Udwary, Sci. Rep. **7**, 9297 (2017).

[16] M. A. Reshchikov, A. A. Kvasov, M. F. Bishop, T. McMullen, A. Usikov, V. Soukhoveev, and V. A. Dmitriev, Phys. Rev. B **84**, 075212 (2011).

[17] M. A. Reshchikov, M. A. Foussekis, J. D. McNamara, A. Behrends, A. Bakin, and A. Waag, J. Appl. Phys. **111**, 073106 (2012).

[18] M. A. Reshchikov, J. Appl. Phys. **115**, 012010 (2014).

[19] M. A. Reshchikov, P. Ghimire, and D. O. Demchenko, Phys. Rev. B **97**, 205204 (2018).

[20] M. A. Reshchikov, J. Appl. Phys. **115**, 103503 (2014).

[21] M. A. Reshchikov, *Internal Quantum Efficiency of Photoluminescence in Wide-Bandgap Semiconductors*, edited by M. A. Case and B. C. Stout (Nova Science Publishers, New York, 2012), pp. 53–120.

[22] J. F. Muth, J. H. Lee, I. K. Shmagin, R. M. Kolbas, H. C. Casey, Jr., B. P. Keller, U. K. Mishra, and S. P. DenBaars, Appl. Phys. Lett. **71**, 2572 (1997).

[23] V. N. Abakumov, V. I. Perel, and I. N. Yassievich, *Nonradiative Recombination in Semiconductors* (Elsevier, Amsterdam, 1991).

[24] M. A. Reshchikov and H. Morkoç, Mat. Res. Soc. Symp. Proc. **831**, E3.7 (2005).

[25] A. Castaldini, A. Cavallini, L. Polenta, C. Diaz-Guerra, and J. Piqueras, J. Phys.: Condens. Matter **14**, 13095 (2002).

[26] E. R. Glaser *et al.*, Physica B **308**, 51 (2001).

[27] M. A. Reshchikov, M. H. Zhang, J. Cui, P. Visconti, F. Yung, and H. Morkoç, Mat. Res. Soc. Symp. Proc. **639**, G6.7 (2001).

[28] D. M. Hofmann, B. K. Meyer, H. Alves, F. Letter, W. Burkhard, N. Romanov, Y. Kim, J. Krüger, and E. R. Weber, Phys. Stat. Sol. a **180**, 261 (2000).

[29] E. M. Goldys, M. Godlewski, T. Paskova, G. Pozina, and B. Monemar, MRS Internet J Nitride Semicond. Res. **6**, 1 (2001).

[30] M. A. Reshchikov and R. Y. Korotkov, Phys. Rev. B **64**, 115205 (2001).

[31] R. Dingle, Phys. Rev. Lett. **23**, 579 (1969).

[32] J. L. Lyons, A. Alkauskas, A. Janotti, and C. G. Van de Walle, Phys. Stat. Sol. b **252**, 900 (2015).

[33] F. Tuomisto, T. Kuittinen, M. Zajac, R. Doradzinski, and D. Wasik, J. Crystal Growth **403**, 114 (2014).

[34] A. Uedono, T. Fujishima, Y. Cao, Y. Zhang, N. Yoshihara, S. Ishibashi, M. Sumiya, O. Laboutin, W. Johnson, and T. Palacios, Appl. Phys. Lett. **104**, 082110 (2014).

[35] E. Malguth, A. Hoffmann, and M. E. Phillips, Phys. Stat. Sol. b **245**, 455 (2008).

[36] U. Gerstmann, A. T. Blumenau, and H. Overhof, Phys. Rev. B **63**, 075204 (2001).

[37] J. Baur, U. Kaufmann, M. Kunzer, J. Schneider, H. Amano, I. Akasaki, T. Detchprohm, and K. Hiramatsu, Appl. Phys. Lett. **67**, 1140 (1995).

[38] J. A. Freitas, Jr., J. C. Culbertson, E. R. Glaser, E. Richter, M. Weyers, A. C. Oliveira, and V. K. Garg, J. Cryst. Growth **500**, 111 (2018).

[39] K. Fujito, S. Kubo, H. Nagaoka, T. Mochizuki, H. Namita, and S. Nagao, J. Crystal Growth **311**, 3011 (2009).

[40] Y. S. Puzyrev, R. D. Schrimpf, D. M. Fleetwood, and S. T. Pantelides, Appl. Phys. Lett. **106**, 053505 (2015).

[41] D. Wickramaratne, J.-X. Shen, C. E. Dreyer, M. Engel, M. Marsman, G. Kresse, S. Marcinkevičius, A. Alkauskas, and C. G Van de Walle, Appl. Phys. Lett. **109**, 162107 (2016).

[42] T. K. Uždavinys, S. Marcinkevičius, J. H. Leach, K. R. Evans, and D. C. Look, J. Appl. Phys. **119**, 215706 (2016).